Turkish Journal of Civil Engineering, 2023 1-42, Paper 731, ***Research Article***

Building's Controlled Seismic Isolation by Using Upper Horizontal Dampers and Stiff Core

Kourosh TALEBI JOUNEGHANI[1]
Mahmood HOSSEINI[2]
Mohammad Sadegh ROHANIMANESH[3]
Morteza RAISSI[4]

ABSTRACT

The fundamental period of the seismically isolated buildings may be close to that of the long period pulses of near-field earthquakes, leading to very large lateral displacements in isolators, which in turn can considerably reduce the stability of isolators, increase the chance of collision of the isolated buildings to adjacent buildings, or even result in overturning of the isolated buildings. Therefore, it is important to control these types of buildings and reduce the amount of lateral displacement in their isolating system. In this study, by conducting a series of time history analyses for a set of five multi-story steel buildings with various numbers of stories from 3 to 14. Each building is considered to have a very stiff core structure and a set of crosswise viscous dampers, connecting the building structure to the core structure at the lowest and the top floors, as well as the same structures without the core structure and dampers. The effect of stiff core and dampers in reducing the lateral displacement at isolators has been shown. Results indicate that by the proposed technique, the lateral displacement of the base isolation system is significantly decreased particularly for low-rise buildings.

Keywords: Control of displacement, base-isolated structures, crosswise dissipators, central rigid support.

Note:
- This paper was received on February 20, 2022 and accepted for publication by the Editorial Board on March 3, 2023.
- Discussions on this paper will be accepted by July 31, 2023.
- https://doi.org/10.18400/tjce/1265467

1 Department of Civil Engineering, Central Tehran Branch, Islamic Azad University, Tehran, Iran
kou.talebijouneghani.eng@iauctb.ac.ir - https://orcid.org/0000-0003-4340-0381

2 Eastern Mediterranean University, Department of Civil Engineering, Famagusta, North Cyprus
mahmood.hosseni@emu.edu.tr - https://orcid.org/0000-0003-3142-4087

3 Department of Civil Engineering, Central Tehran Branch, Islamic Azad University, Tehran, Iran
m.s.rohanimanesh@iauctb.ac.ir - https://orcid.org/0000-0002-8426-8906

4 University of Science and Technology, Department of Civil Engineering, Tehran, Iran
mraissi@iust.ac.ir - https://orcid.org/0000-0003-2364-1268

1. INTRODUCTION

Considering the significant interest in structurally controlling the base-isolated buildings, the fundamental model for a specific type of building was established in [1] and [2]. The eight-story building had a length of 82.4m and a width of 54.3m, a replica of a structure in Los Angeles. The model package is a result of the cooperative study between various researchers. Hence, a realistic and detailed 3D modelling was obtained for a base-isolated building model. Researchers could use an exact structural model to compare and design numerous control systems. Various controllers were utilized during the Engineering Mechanics Conference (Newark, Delaware, June 2004), and different investigators contributed to the benchmark study and provided their preliminary results [3–10].

Recognizing the importance of earthquake improvement and building retrofitting and attempts to achieve these goals is of great concern for many researchers. Seismic isolators and viscous dampers rank as two of the most effective solutions among these techniques. These gadgets differ from one another in that each has benefits and drawbacks. Dampers are tools for releasing energy generated by an earthquake inside a building. There are many different kinds of dampers, but viscous dampers are particularly popular because of their simple installation and extended lifespan [11–14].

Seismic isolators with significant lateral deformation capability support the building. When there is an earthquake, the column often bears the brunt of the displacements, with the rest of the building functioning more like a solid object oscillating with minor displacements. By extending the time and dampening the structure, installing an isolator causes seismic loads to decrease rather than improve the structure's bearing capability. Active, passive, and semi-active control systems, which employ techniques other than enhancing the structure's strength and capacity, might be noted among the methods for regulating the reaction of structures. They reduce the force on the structure during an earthquake. For example, vibration isolation systems increase the natural period and damping of the design and effectively reduce the force on the structure. This isolation is achieved by increasing the system's flexibility and providing proper damping. In this method, since the force of the earthquake is not supposed to enter the structure or a small part of it is transferred to the structure, it can be expected that the displacement of the floors will be reduced, the acceleration of the floor will be reduced, and the failures of the building and also the failures of the property will be significantly reduced. Moreover, fewer architectural problems will arise in the plans, and the cost of implementing huge structures will decrease due to the use of finer sections [15, 16]. According to the functioning of isolation systems, the use of these systems in soils with low shear wave velocity (soft), although they increase the damping of the entire system and, as a result, less energy is introduced into the structure, but due to the increase in the need to change the location that one of the main criteria for using these systems is that it always faces limitations. Therefore, the need to change location and move a lot in earthquakes near the fault due to the frequency content and special features of these records is one of the limitations of this system [17]. In recent years this issue may have been solved to some extent with additional dampers added to the isolation system, especially in bridges [18]. Wu et al. [19] studied the failure of structures on sandstone and mudstone. In another study [20], they numerically studied water inrush from rock strata separation space. However, the research on the effects of these dampers on isolated systems is one of the essential issues in this research on the damping effect of viscose add-on dampers in isolated structures. The seismic

isolation of buildings was aimed at saving the structure and avoiding damage to the contents, including its residents [21, 22]. The superstructure response is reduced by base isolation systems like elastomeric bearing systems and sliding.

However, the base displacements were increased in near-fault earthquakes. Recently, many studies have been devoted to limiting bearing displacements. Protecting the base-isolated buildings from long-period and intense pulses in near-field earthquakes is challenging. Heaton et al. [23] showed that large drifts were observed in a near-field earthquake in a base-isolated building. Rupture or buckling of the isolation bearings was noted when the structure was subject to a strong earthquake [24, 25]. However, isolator displacements are reduced by large damping levels in the fundamental mode since forces are imparted into the structure, thus, increasing the structural deformations and accelerations in higher modes [26, 27]. Different kinds of systems were proposed to address the requirement for higher damping and limit the low damping and isolation drift to enhance the isolation effectiveness at higher frequencies.

Detailed reviews have been provided on the studies on structural response control [28-33]. In active structural control, the control force is straightly exerted on the model in terms of a definite algorithm. For this purpose, to obtain certain response control objectives under the device capacity limitation, state estimation or response measurements are used along with direct actuation tools (hydraulic actuators). Among other benefits of active control systems are applicability to multi-risk situations (such as wind and earthquakes), relative insensitivity to site circumstances and ground motions, and selectivity of control objectives like safety during severe dynamic loading and human comfort during non-critical times. Wu et al. [34] studied the deformation and failure of structures using convolutional neural networks.

Seismic excitations are traditionally ignored or assumed as white noise in designing optimal active control systems. Therefore, it is impossible to guarantee these 'optimal' controllers' optimality while existing seismic excitations have significant pulse performance. Yang [35] recommended designing controllers in terms of the augmented system, including the filter and the structure, to model filtered white noise. He used the same method to control the nonlinear hysteretic structures [36]. Various studies propose other structural control methods [37-45]. Optimal structural control was proposed by Panariello et al. [46] by conducting an experiment using artificial neural networks. In order to design a smart base isolation system, Yoshioka et al. [47] and Ramallo et al. [48] modelled the earthquake excitations by using Kanai–Tajimi filter [49]. For the input shaping filter, the recorded earthquake's PSD is fitted with a second-order transfer function to obtain the transfer function. The shaping filter of Kanai–Tajimi was employed by Ramallo et al. to model the ground. Thus, the structural excitation augmented system is obtained to design an MR damper controller. Using filters from [50] for modelling input excitation was proved to be the overall result. However, these filters overestimated the energy within the lower frequency range while affecting the longer-period structures' response. Nagarajaiah and Narasimhan [2] proposed a modified model [38]. A lower overestimating is achieved for energy by the modified model within the lower range of frequency in comparison with the original model. He [51] and He and Agrawal [52] proposed an analytical model for control systems in near-field ground motions [53]. He and Agrawal extensively studied the use of the analytical pulse model for the benchmark cable-stayed bridge model [54]. A frequency-domain pulse filter was established by converting the analytical pulse model in the Laplace domain. An active pulse filter (APF) controller can be

designed by further augmentation of the pulse filter into state-space form through the structural system [55]. APF (Active Pulse Filter) is the name of the active controller. To conduct a parametric study independent of noise disturbances, the measurement of noise disturbances hasn't been considered when designing and simulating controllers in this paper. APF controllers are however investigated in [55-57] for their effects on white noise disturbances. APF controllers have been shown to be robust according to simulation results in the benchmark package for base-isolated buildings [2].

A previous study determined that weighting parameters in semi-active and active control algorithms such as Linear Quadratic Regulators (LQR) and H2/LQG are constant during earthquake loading, while in the MH2/LQG control algorithm, a variable weighting parameter is considered at each time step for the purpose of designing the semi-active control system and determining appropriate damper forces for the MR. The MH2/LQG control algorithm adjusts the weighting parameter at time steps where the MR damper is not required to apply excessive damping forces to the structure in order to prevent this.

According to some seismologists, buildings that are isolated from the base may be subject to significant impulsive ground movements that are produced by nearby faults. Large insulator displacements caused by long-period pulses linked to movement near the fault might cause the buildings that are separated from the base to operate poorly. Researchers were quite interested in this, and lately, several studies have been published on the dynamic behavior of base-insulated structures during near-fault motions [58]. It has been shown that bearing displacements in near-fault motions can be quite considerable, which can cause the isolation system to become unstable. According to the research above, the LRB (Lead Rubber Bearings) system's performance with specific attributes was unsuitable for movements close to faults. Since the LRB system is a popular isolation system with all the features needed for fundamental isolation, it is important to research how the LRB system behaves dynamically and what its best settings are when the fault is moving [58].

This study presents the method of using four cross-horizontal viscous dampers at the level of the roof of the structures, which is connected to a rigid central core in the center of the structures. Also, they are equipped with seismic isolators to restrain the lateral displacement of the structures under the effect of pulses in the near field.

2. MODULATION

In this research, five types of 3, 5, 8, 11, and 14-story steel bending frame structures with Chevron braces with square plans have been designed using ETABS 2016 software using the LRFD method. Then, for each building, rigid concrete central support structure was designed using ETABS 2016 software and transferred to the Perform3D simulator software.

Then, in this software, base isolators and specific horizontal viscous dampers are added to the structures. Each type of building is divided into two categories. The first category is equipped with a base isolator without a hard-central support structure, and the second category is equipped with a base isolator with a hard-central support structure. These structures have been subjected to nonlinear dynamic analysis under seven distant and seven near-earth records. The outputs of all structures have been examined, and the following results have been obtained.

2.1. Designing the Structures

All the structures have a Chevron brace and have a yard to establish the supportive structures. The design of the structures was performed by the AISC 360-05 [59] LRFD technique and UBC-97 in ETABS 2016 Provided Seismic zone factor (Z) =0.4. The load combinations under Strength level (U) =1.2D+0.5L+E were used, where D, L and E are dead load, live load, and lateral load, respectively. Site soil profile types are (stiff soil profile) by the shear wave velocity 180 to 360 meter/second. ST37 type steel is used for all structures with 370 mega Pascal ultimate tensile strength. They were then transported to PERFORM3D to analyze the nonlinear time history. The types of structures are shown in Fig. 1, and the section properties are given in Table 1.

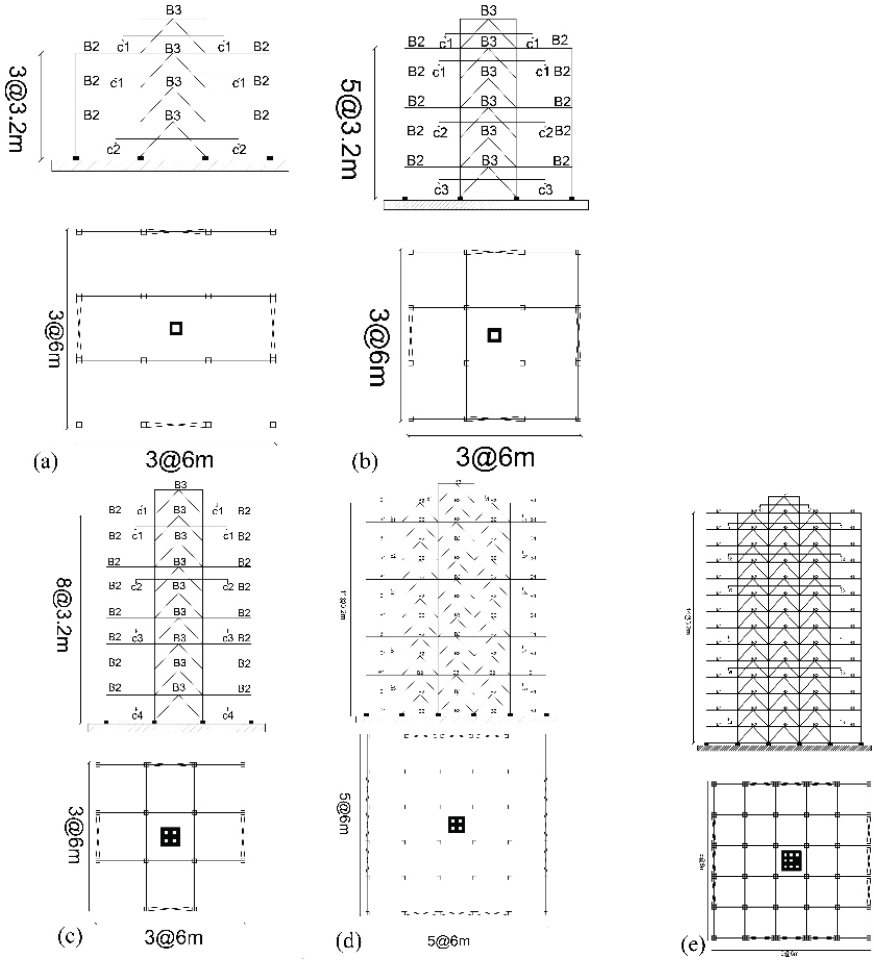

Fig. 1 - The structures with no rigid support of (a) 3 stories, (b) 5 stories, (c) 8 stories, (d) 11 stories, and (e) 14 stories

Table 1 - Section properties for Fig. 1.

Column section		**Beam section**
$B \times t\ (cm)$		$[(h_w \times t_w) + (b_f \times t_f)]\ \ (cm)$
$c_1 = 35 \times 2$	$c_4 = 50 \times 3$	$B_1 = (40 \times 1) + (20 \times 1.5)$
$c_2 = 40 \times 2.5$	$c_5 = 60 \times 3.5$	$B_2 = (45 \times 1.5) + (25 \times 2)$
$c_3 = 45 \times 3$	$c_6 = 80 \times 5$	$B_3 = (50 \times 2) + (30 \times 3)$
$B = width$		$t_w = web\ thickness$
$t = thickness$		$b_f = flange\ width$
$h_w = web\ height$		$t_f = flange\ thickness$

2.2. Designing the Stiff Core (Rigid Support Structure)

The current survey of the United Nations approximated that more than half of the people accommodate in cities [60]. Furthermore, it was also estimated that more people will be living in the cities by the end of 2050. Therefore, the number of houses and apartment complexes is rising in urban areas. Normally, tall buildings are more susceptible to wind actions and ground motions than low-rise buildings. Hence, effective lateral force-resisting systems should be used to reduce lateral demands. In order to solve this problem, reinforced concrete (RC) is utilized in high-rise structures. This provides the benefits of flexible architecture, faster construction, and commodious area [61].

The columns in an RC-supported structure have the flexibility to transfer the gravity loads. One of the most accurate and precise numerical approaches is the nonlinear response history analysis (NLRHA) process, which computes the high-rise structures' dynamic responses. However, it is computationally expensive, time-consuming, and needs expertise in nonlinear modelling. Mehmood et al. [62] revealed that the NLRHA procedure requires a computation time of about 30 hours for predicting a building's seismic responses for a certain case. Moreover, another 5 hours is required for the post-processing. Thus, various simplified analysis processes have been developed to avoid the issues related to the NLRHA process. Nonlinear modelling is required by some of the simplified processes, while the linear elastic modelling option is served for others. However, these approaches have less accuracy in comparison to the NLRHA technique. The simplified techniques were mostly adopted in different codes [63-65]. Recently, more analysis processes have been proposed [66-73]. However, the present study has concentrated on more developed models.

No study exists examining the simplified procedures, particularly for high-rise core wall buildings. The present study is aimed to compare all the simplified methods for their computational efforts, computation time, and relative accuracy for high-rise core wall structures. It provides the demerits and merits of different simplified analysis procedures in detail. Moreover, a modified simple analysis procedure is presented using modal decomposition methods based on an in-depth analysis of modal responses.

The rigid support structure is a central square core wall with high-strength steel (HSS) with 650 mega Pascal ultimate tensile strength and high-strength concrete (HSC) with 60 mega Pascal compressive strength. It was designed via the ACI 363R-92 [74]. This structure is connected rigidly to the foundation. Moreover, by horizontally crosswise viscous dampers, the structures are linked to the support structure in the roof, as shown in Fig 2.

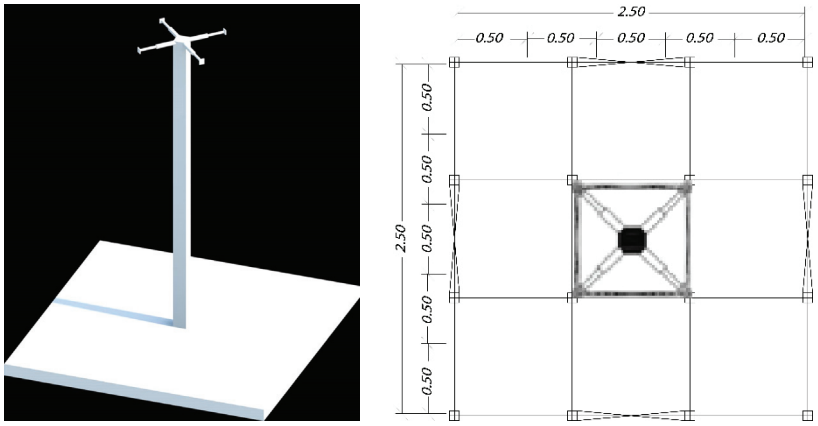

Fig. 2 - Schematic configuration of rigid support structure

Fig. 3 shows the details of the support system.

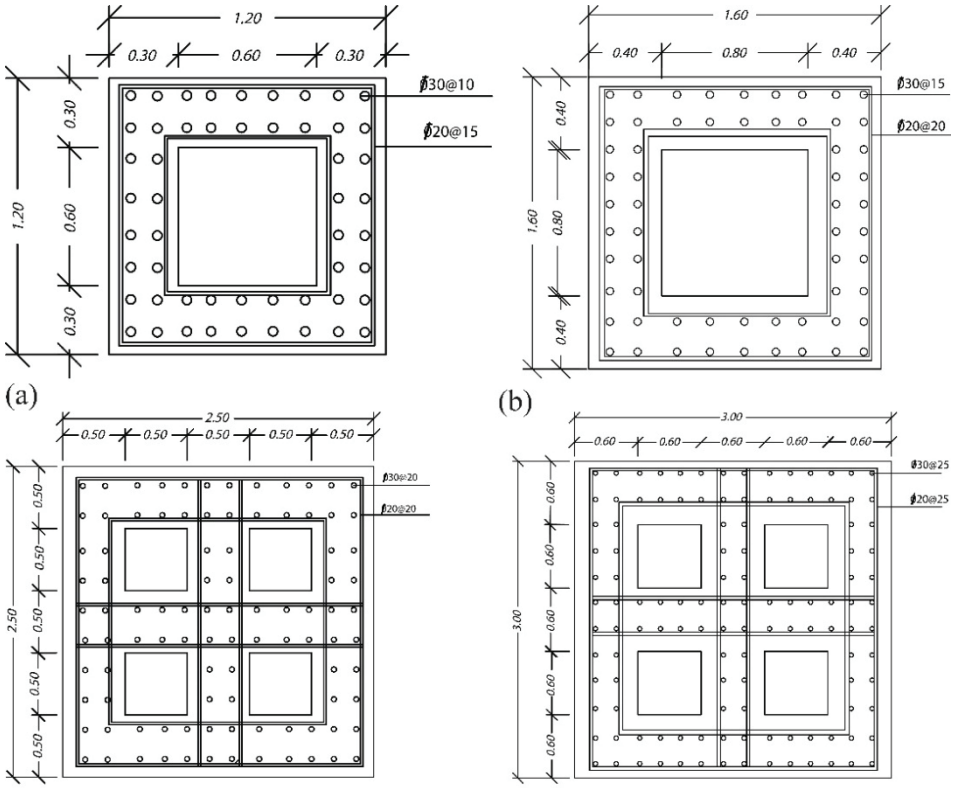

Fig 3 - The details of rigid supports for (a) 3 stories, (b) 5 stories, (c) 8 stories, (d) 11 stories, and (e) 14 stories

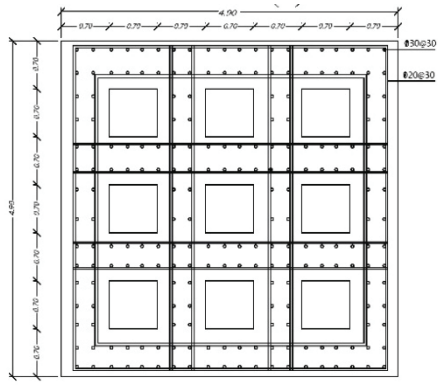

Fig 3 - The details of rigid supports for (a) 3 stories, (b) 5 stories, (c) 8 stories, (d) 11 stories, and (e) 14 stories (continued)

2.3. Base Isolation System

Among the influencing parameters in the response of isolated structures under near-field earthquakes, we can mention the important feature of LRB isolators, i.e., the stiffness ratio before and after yielding of rubber isolator with lead core, B_{ratio}. To investigate the effect of that parameter, it is considered as a variable to determine the value of the minimum response of the isolated structure under the influence of the nearby earthquake [75].

In this study, Wen and Bouc models are used for nonlinear modelling and expression of the hysteresis behavior of the LRB system [75].

One of the influential parameters in the response of the isolated system is the amount of damping of the isolated system with the behavior of the linear displacement force. Increasing the damping controls the deformation of the structure, but on the other hand, it increases the acceleration of the structure. Therefore, two parameters of acceleration and displacement of the separator system were studied simultaneously under near-field accelerometry. For this purpose, the structure with frequency characteristics ω_s, period T_s, and damping ς_s and separator with frequency characteristics ω_b, period T_b, damping ς_b and $\gamma = \frac{m}{(m+m_b)}$ were investigated [76].

Another important parameter in the response of the system under an earthquake is the normalized yield strength F_0 of the LRB isolator, which has been studied in [77]. For this purpose, an N-story building equipped with an LRB isolator was used. The yield strength parameter is normalized and is defined according to equation 1.

$$F_0 = \frac{F_y}{W} \tag{1}$$

where F_y is the yield strength of the isolator, and W is the total weight of the isolated building. For more detail, in this regard, the study of Jangrid [77] is introduced.

The LRB yield strength ought to be such that it offers sufficient initial rigidity when there is no yielding in the lead core because, for relatively small values of the isolator yield strength, the efficient period of the isolated building is around 2.5 seconds, which is extremely similar to the interval time of the isolator pulse [77].

It can be said that in the design of the LRB separator, the optimal value for the LRB is slightly higher than the F_0 related to the acceleration of the minimum floors in order to achieve the maximum amount of separation with the least amount of floor displacement. This value of F_0 is considered to be about 0.1 to 0.15.

Typically, there are two kinds of seismic isolators, which are sliding bearings [78] and [79] and rubber bearings (LRBs) [80]. As previously stated, the present work aims to assess the effects of viscous dampers and lead rubber bearings' performance concerning the features of the near-field ground motion. The LRB isolator is able to neutralize the impact using a particular hysteretic lead plug. Thus, it supports the structure vertically and offers limited horizontal autonomy. The designed isolators of the present study are based on the Uniform Building Code (UBC-97) [80]. The present study's design parameters are introduced in Table 2.

Table 2 - The design parameters used in the present study

Parameter	Details
Q/W	The ratio of the characteristic strength to the total weight on the isolation system
D	The isolator diameter
F_y	The yield force
n	The number of rubber layers
d	The lead core diameter
t	The layer thickness

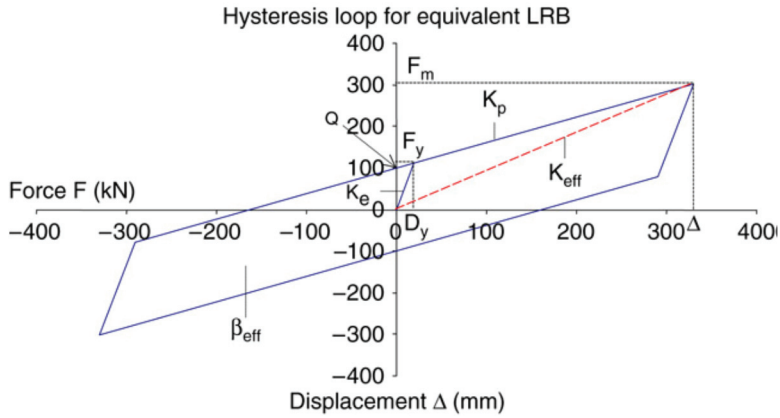

Fig. 4 - The typical bilinear LRB hysteresis

Fig. 4 demonstrates the bilinear curve used for analysis purposes in the present study. It specifies k_e and k_p which are the elastic and post-yield stiffness, respectively.

k_e and k_p are determined as follows:

$$k_e = \frac{F_y}{D_y} \tag{2}$$

$$k_p = \frac{G.A_r}{t_r} fL \tag{3}$$

where, D_y, G, and A_r are the yield displacement, the shear modulus, and the cross-sectional area of rubber, respectively. fL is a constant, which is set to be 1.5. The strength is also calculated by:

$$Q = A_{pb}\sigma_{y_{pb}} \tag{4}$$

where, A_{pb} and $\sigma_{y_{pb}}$ are the area and the yield strength of the lead core, respectively. Furthermore, the effective stiffness k_{eff} is calculated as follows:

$$k_{eff} = \frac{F_m}{\Delta} \tag{5}$$

where, F_m is the force and Δ is the displacement. The effective stiffness is also calculated as Eq. 6.

$$k_{eff} = \begin{cases} k_p + \frac{Q}{\Delta} & (if\ \Delta > D_y) \\ k_e & (if\ \Delta < D_y) \end{cases} \tag{6}$$

Also, the forces are formulated as:

$$F_m = Q + k_p\Delta \tag{7}$$

$$F_y = Q + k_p D_y \tag{8}$$

The area ED of the hysteretic loop, which corresponds to the amount of dissipated energy, is obtained as:

$$ED = 4Q(\Delta - D_y) \tag{9}$$

The amount of hysteretic energy that is dissipated by the isolator is defined as the effective damping ratio ζ_{eff}.

$$\zeta_{eff} = \frac{ED}{2\pi k_{eff}\Delta^2} \tag{10}$$

Ultimately, the fundamental isolation period T^{iso} is achieved as:

$$T^{iso} = 2\pi\sqrt{\frac{M}{\sum K_{eff}}} \tag{11}$$

M is the overall mass of the system. Fig. 5 shows the hysteretic curves for different cases.

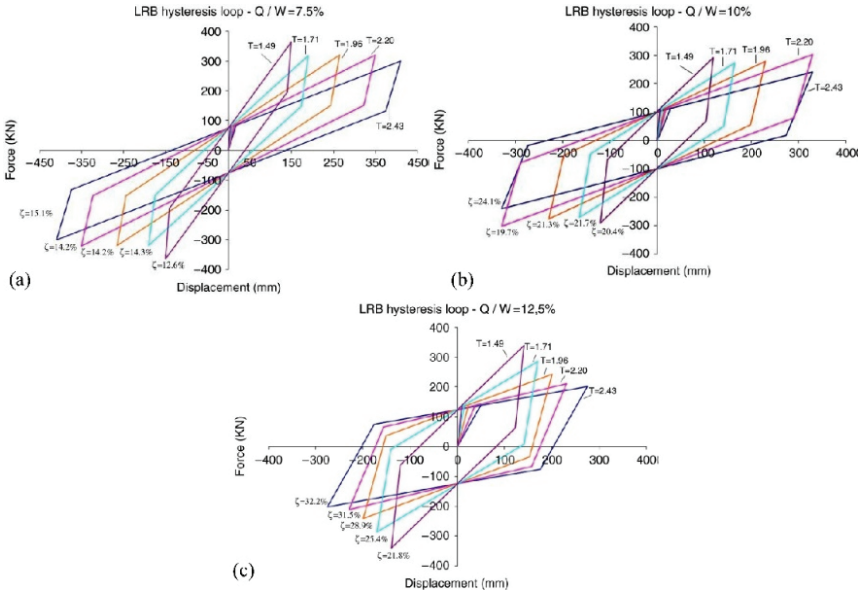

Fig. 5 - The LRB isolators hysteretic curve for the cases of (a) $Q/W = 7.5\%$, (b) $Q/W = 10.0\%$, and (c) $Q/W = 12.5\%$

The equation of motion is utilized to determine the maximum deformation of the isolation system to calculate the initial values [81]. This approximation of the maximum deformation is accurate [82].

$$M\ddot{x}_b(t) + C_{eff}\dot{x}_b(t) + K_{eff}x_b(t) + \sum_{q=1}^{Q} m_q a_q = -M\ddot{x}_g(t) \tag{12}$$

Where, Eq. 12 is the equation of motion. $\ddot{x}_g(t)$, $x_b(t)$, m_q, a_q, and Q are the horizontal ground acceleration, the relative displacement of the isolator, mass, relative acceleration of the nth degree of freedom, and the number of superstructure's degrees of freedom, respectively.

C_{eff} is the effective damping coefficient which is formulated as follows:

$$C_{eff} = 2\zeta_{eff}\sqrt{MK_{eff}} \tag{13}$$

Fig. 6 and Table 3 provide the properties of the isolators used in PERFORM3D.

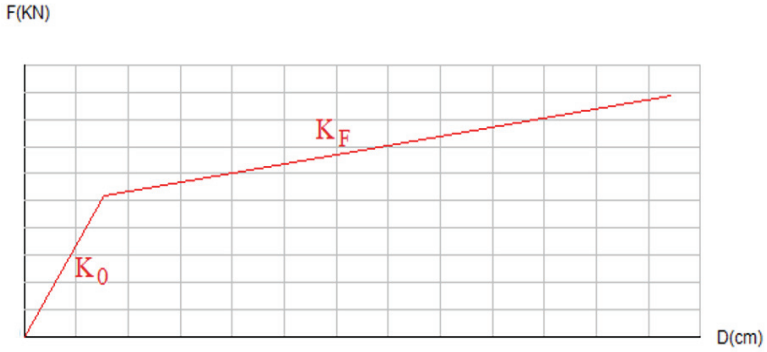

Fig. 6 - Force-displacement relationship for lead rubber bearing

Table 3 - The relationship of force/displacement for lead rubber bearing for T=2.43

Structures	$K_e = K_o$ **(KN/M)**	D_{max} **(mm)**	F_u **(KN/M)**	$K_p = K_F$ **(KN/M)**
3 story	400	400	14	0.200
5 story	485	485	16.5	0.225
8 story	530	530	19	0.255
11 story	605	605	22.5	0.311
14 story	675	675	26	0.311

Note that in Perform3D, K_e and K_p are introduced as K_o and K_f.

2.4. The Fluid Viscous Damper System

Viscous fluid dampers are frequently used as energy dissipation tools to protect structures from earthquakes. These dampers are made of a hollow cylinder filled with fluid, usually silicone-based fluid. Strong forces opposing the damper's relative motion can be produced by the pressure difference across the piston head [82]. Heat is produced as a result of energy dissipation caused by friction forces. When the damper is exposed to lengthy or large-amplitude vibrations, the resulting temperature increase can be severe [83, 84]. There are mechanisms to counteract the temperature increase such that the impact on damper behavior is minimal [85]. The possibility of heat-related harm to the damper seals increases the temperature [84]. Strangely, even though the damper is referred to as a viscous fluid damper, the fluid often has a low viscosity, such as silicone oil, which has a kinematic viscosity of around 0.001 m^2/s at 20°C. The phrase "viscous fluid damper" refers to a damper's macroscopic behavior, nearly identical to that of an ideal linear or nonlinear viscous dashpot in that the resistive force is proportional to the velocity.

Viscous dampers present a resisting force to the velocity [86, 87]. In order to calculate the damper force, we use Eq. 14.

$$F_D = cV_c^{exp} \quad (14)$$

Where, c and V_c are the coefficient and the relative velocity. Also, exp is a constant ranging from 0.1 to 0.3. In the present study, the mentioned parameter is set to 1 for simplicity. Fig. 7 presents the relation between the applied force and the displacement of the viscous damper.

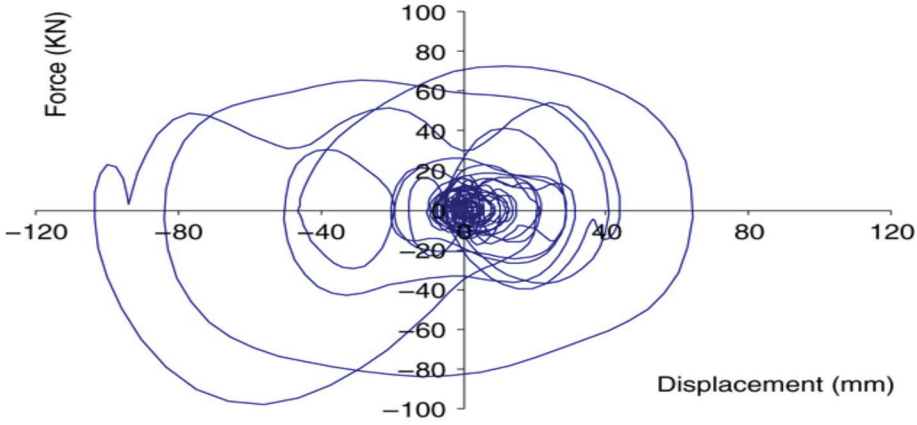

Fig.7 - The typical relation of the force and the displacement in a viscous damper

The viscous damper's parameters are represented in Fig.8.

Fig. 8 - The force-displacement association for fluid and the viscous damper in a structure with 3 stories

The axial force in the viscous damper is calculated by:

$$Axial\ Force = C\ (Deformation\ rate)^{0.5} \quad (15)$$

The coefficient of each structure based on its number of stories and the force in the last segment is given in Table 4.

Table 4 - The value of C under different conditions (number of stories and the force at last segment)

Segment	Deformation rate	3 stories 20,000 Kgf	5 stories 40,000 Kgf	8 stories 60,000 Kgf	11 stories 80,000 Kgf	14 stories 100,000 Kgf
1	0.6	2222	4444	6667	8889	8889
2	2.4	1333	2667	4000	5333	5333
3	5.4	952.4	1905	2857	3810	3810
4	9.6	740.7	1481	2222	2963	2963
5	15	606.1	1212	1818	2424	2424

Regarding the equation of motion, a thorough explanation is given in our previous research [88-90], and the reader is referred to those papers.

2.5. Ground Motion Information

Ground motion components should be matched and scaled based on the design spectrum to avoid scattering the time history analysis results. The design spectrum is determined based on the ground motions components of the construction site and according to the hazard and soil characteristics in different site layers with a damping value of 5%. Initially, each record is scaled based on the maximum Peak Ground Acceleration (PGA) of gravity of the earth (g). Each scaled record's response spectra are calculated with a 5% damping value. The square root of the sum of squares (SRSS) of each response spectra was determined. The average of SRSS in the range of 0.2T to 1.5T of all the earthquakes under study is calculated (T is the fundamental period of the structure), and this number, which is the coefficient of scale, is introduced to the software. This average should not be less than 1.17 times the design spectrum. According to the national regulations of the building, the selected records must be in harmony with the desired building in terms of size, fault mechanism, and the distance from the fault to the place of registration. If the required records do not exist, modified or artificial records can be used. The number of records used and how to modify the records to match the existing conditions are important questions. For this research, earthquake records were selected based on FEMA P695 recommendation, where 22 earthquake records for the distant area and 28 records for the near area were mentioned.

In comparing spectra and codes of earthquakes, the desired return period should be the same for response spectra and the design spectrum of codes. In other words, to check each earthquake's effect on the structure and evaluate the tremors of the buildings, it is necessary that the response spectra be adapted or scaled with the spectra of the corresponding plan to a specific return period. SeismoSignal software was used for scaling, and all records were scaled for all modes.

Individual recorded events must be scaled and selected to determine the horizontal components of the ground motion. It is appropriate to use ground motions whose magnitudes, fault distances, and source mechanisms are consistent with those controlling the maximum earthquake considered. Whenever there are not enough recorded ground motion pairs to fulfill the requirement, simulated ground motion pairs will be used as a substitute to fulfill the requirement. The square root of the sum of squares (SRSS) spectrum for each pair of

horizontal ground motion components will be calculated by taking the SRSS spectra of five percent damped response spectra (where the same scale factor will be applied to both components of each pair).

In this study, the two methods of comparing the acceleration are the methods presented in the ASCE07-10. Each pair of acceleration maps must be scaled to their maximum value; for example, we have two acceleration maps of Tabas's earthquake with PGAs of 0.85 and 0.86. First, we multiply both records by a factor of 1/0.86= 1.16. The larger accelerometer's PGA equals 1g (the accelerometer numbers were based on a coefficient of g). And the record with a lower PGA will have a PGA equal to 0.98 (In the third edition of the 2800 standard, the amount of PGA in both acceleration maps was equal to one, which was changed in the fourth edition). In the SeismoSignal software, according to each couple, we extract the accelerometer scaled to the maximum with 5% damping. We obtain the response spectra of each map acceleration pair in each period by the root sum of squares method. In the range of 0.2T to 1.5T (where the period is the main), we get the root mean of the sum of squares. Important: only in the three-dimensional analysis should this average not be more than 10% less than 1.3 times according to the plan; that is, it should be more than 1.17 times the spectrum of the plan. The coefficient obtained in this way is entered as a scaling coefficient in the software.

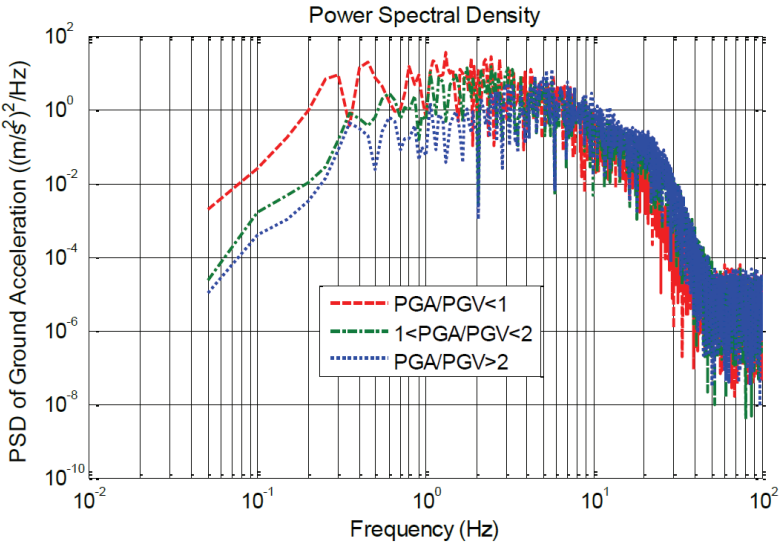

Fig. 9 - The power spectral density of different earthquakes

The ground motions whose PGA/PGV is smaller than one have been selected because of their highest intensity (Fig. 9). Table 5 illustrates the ground motions, and Figure 10 shows the spectral acceleration of the ground motions together with their mean.

Table 5 - The characteristics of different ground motions (PGA/PGV)

Earthquake Name	Year	Duration time	PGA (g)	PGV (m/s)	PGD (m)	PGA/PGV
TCGH13	2004	21	0.590	0.626	0.098	0.945
KOBE	1995	50	0.834	0.911	0.211	0.915
Imperial Valley-02	1940	55	0.280	0.309	0.087	0.905
Tabas	1978	40	0.027	0.034	0.31	0.768
Tabas	1978	33	0.861	1.234	0.936	0.698
Bam	2003	33	0.014	0.020	0.013	0.696
Imperial Valley-02	1940	55	0.210	0.313	0.241	0.670
El Mayor-Cucapah	2010	130	0.248	0.383	0.482	0.648
Northridge	1994	28	0.426	0.748	0.190	0.569
Kocaeli	1999	150	0.045	0.081	0.035	0.555
Tottori	2000	120	0.018	0.036	0.042	0.511
Duzce	1999	95	0.017	0.045	0.038	0.373
Northridge01	1994	30	0.410	1.114	0.446	0.368
Darfield	2010	140	0.194	0.591	0.491	0.328
Zealand	2010	120	0.209	0.671	0.599	0.311

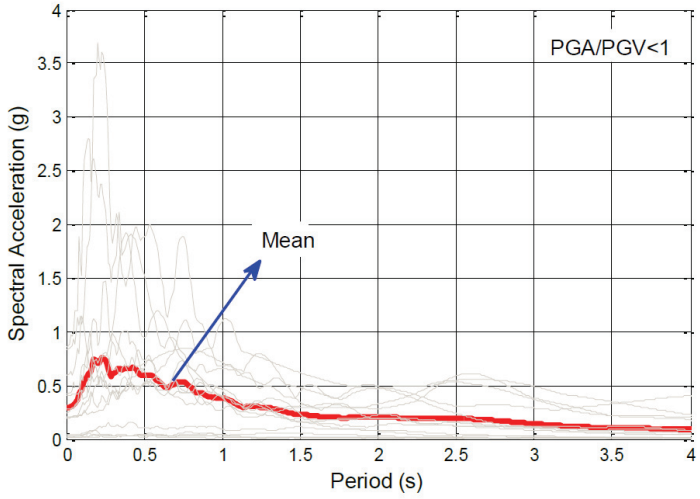

Fig. 10 - 5% damped acceleration spectra if the selected ground motions

The SeismoArtif software was used to create fake earthquakes based on the median spectrum ground movements in Fig. 10. (version 2018). The Saragoni and Hart [91] envelope curve approach was applied while considering the following requirements (Fig. 11).

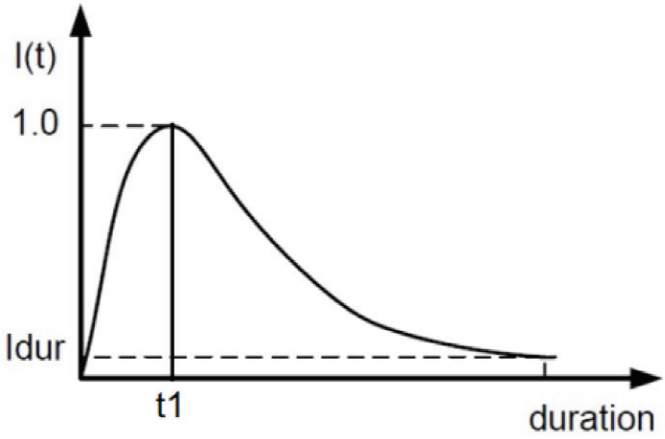

Fig. 11 - Saragoni and Hart envelope curve [91]

By executing the procedure mentioned above, it can be seen from Fig. 12 that the actual spectrum matches the specific target spectrum with 5% damping.

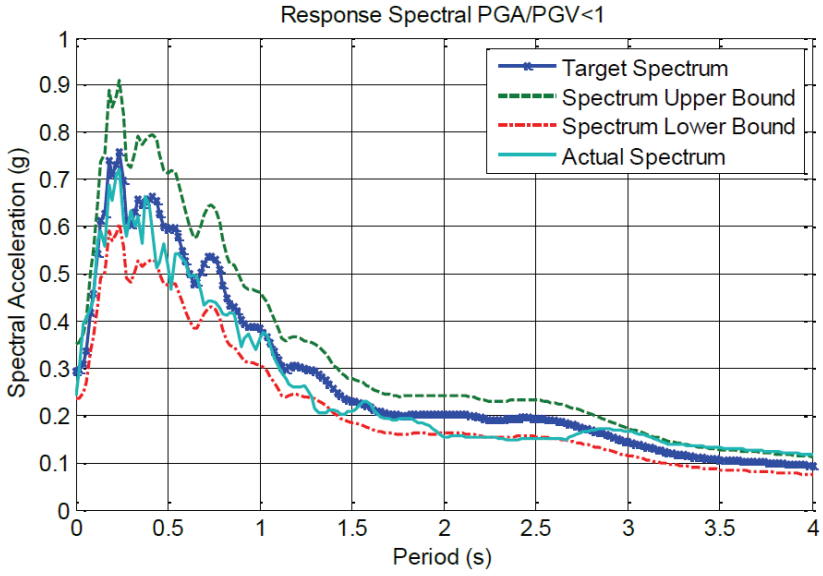

Fig. 12 - The response spectral matched the target spectrum

Tables 6 and 7 present the 7 near-field (N.F) and 7 far-field (F.F) ground motions used in the current study.

Table 6 - The features of N.F earthquake motions

No.	Earthquake	M	Station	Distance(km)	PGA(g)	PGV(cm/s)	PGD(cm)
1	Northridge	6.69	LA Dam	11.79	0.576	77.09	20.1
2	Chi Chi	7.62	TCU068	3.01	0.5	277.56	715.8
3	San Fernando	6.61	Pacoima Dam	11.86	0.827	34.43	18.67
4	Palm springs	6.06	North Palm springs	10.57	0.669	73.55	11.87
5	Kocaeli	7.4	Sakarya	3.2	0.41	82.05	205.9
6	Gazil	6.8	Karakyr	12.82	0.599	64.94	24.18
7	Whittier narrows	5.99	Santa-fe springs	11.73	0.398	23.75	1.76

Table 7 - The features of F.F earthquake motions

No.	Earthquake	M	Station	Distance(km)	PGA(g)	PGV(cm/s)	PGD(cm)
1	Imperial Valley	6.53	Brawley Airport	43	0.158	36.09	22.63
2	Loma Prieta	6.9	Richmond City Hall	87.87	0.124	17.34	3.58
3	Tabas	6.8	Tabas	55.24	0.851	121.22	95.06
4	Kobe	6.9	KJMA	18.27	0.854	95.75	24.56
5	Chi Chi	7.62	TCU065	26.67	0.831	129.55	93.85
6	Kocaeli	7.51	Sakarya	33.24	0.376	79.49	70.56
7	Northridge	6.7	Huntington BchWaikiki	69.5	0.086	5.01	1.63

3. SIMPLIFIED MODEL

In order to evaluate the performance of a base isolation construction, a single-degree-of-freedom (SDOF) model is suggested. A complete representation of this model is presented in Fig. 13.

The parameters needed for this procedure are shown in the following equations. The simplified SDOF model's mass, starting stiffness, yield deformation, and damping coefficient are denoted by the letters M_e, k_e, d_{ye}, and c_{main}, respectively.

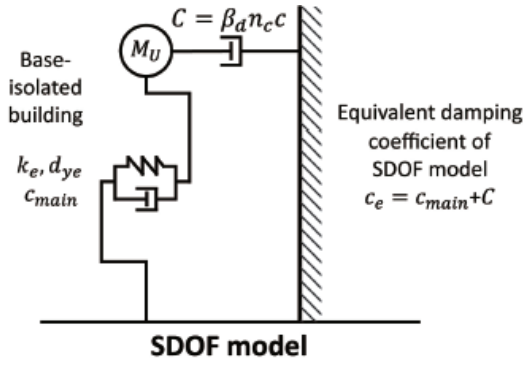

Fig. 13 - A Schematic of the reduced SDOF model

$$M_e = M_U \tag{16}$$

$$k_e = \frac{1}{\left(\frac{1}{k_I}+\frac{1}{k_U}\right)} \tag{17}$$

$$d_{ye} = \frac{K_I d_{yI}}{k_e} \tag{18}$$

$$\frac{1}{k_e+i\omega_e c_{main}} = \frac{1}{k_I+i\omega_e c_I} + \frac{1}{k_U+i\omega_e c_U} \tag{19}$$

$$\omega_e = \sqrt{M_e/k_e} \tag{20}$$

$$c_{main} = \frac{(k_I c_U+k_U c_I)(k_I+k_U)-\left(k_I k_U-\omega_e^2 c_I c_U\right)(c_I+c_U)}{(k_I+k_U)^2+\omega_e^2(c_I+c_U)^2} \tag{21}$$

β_d is the effect of the damper location.

$m_U\ (kg)$	1.70×10^6
$c\ (Ns/m)$	5×10^6
$k_l\ (N/m)$	2.61×10^6
$d_{yl}\ (m)$	0.01

In the design of isolators, performance point methods (PPM) are employed. Depending on the location of the building, spectral acceleration, and displacement are plotted for the 5 percent damped spectrum. In order to decrease the spectrum, equal viscous damping is considered. The isolation system is considered to be dampened by 15 percent in this section. Using the PPM method, the design spectrum has been changed in terms of force-displacement rather than acceleration displacement in light of the bilinear behavior of the isolator. Essentially, bilinear behavior refers to earthquake capacity, while force-displacement

spectrum refers to earthquake demand. A point should be identified in the PPM by plotting capacity and demand together in a diagram. The acceleration-displacement spectrum of the classified isolator is multiplied by 1601 kN, 957 kN, and 511 kN to create three force-displacement spectrums. By intersecting the demand and capacity curves, we are able to reach the isolator design parameters. To begin with, the period, damping, and characteristic strength were assumed, and iterations continued until the desired performance level was reached. Despite the fact that all parameters are the same as those defined in the previous section, post-elastic stiffness (K_2) is calculated based on the isolation period (T_{iso}).

4. NUMERICAL STUDY

This study used accelerograms related to the 7 scaled N.F and 7 scaled F.F earthquakes. Structure motion equations without controller and structure motion equations with central rigid support have been nonlinear time history analyses by PERFORM-3D. The average displacement of the base isolation upper level and stories velocity and acceleration were influenced by 14 earthquakes. These values are presented without a controller and with a central rigid support controller.

4.1. Results and Discussion

Table 8 shows the average absolute value of lateral displacement of the base isolation upper level in structures with and without rigid support. As seen in Table 9 and Table10, the structures' response followed by the time history analysis is extracted under far and near field scaled earthquake scaled records. Therefore, the decreased quantities in the most displacement of the base isolation upper level are presented in the following tables.

Table 11 shows the average absolute value of base shear of the base isolation's upper level in structures with and without rigid support under N.F and F.F earthquakes. As seen in Table 12 and Table13, these structures have the response as discussed in the former section. Moreover, the decreased quantities in the highest base shears are presented.

Table 8 - The average absolute value of lateral displacement of the base isolation upper level in structures with and without rigid support in N.F and F.F earthquakes (cm)

Field / Structure	N.F		F.F		D_{max}
	With rigid support	Without rigid support	With rigid support	Without rigid support	
3 stories	17	3.9	17.5	7.3	40
5 stories	10.8	1.55	19.6	1.82	48.5
8 stories	13.2	2	9.8	1.95	53
11 stories	14.5	3.7	17.9	9.9	60.5
14 stories	7.4	0.95	11.7	3.6	67.5

Table 9 - The percentage of decreased quantity of the lateral displacement of the base isolation upper level in structures with support under N.F earthquakes

Earthquake / Structure	Chi Chi	San Fernando	Palm springs	Kocaeli	Gazil	Whittier narrows	Northridge
3 stories	89.1	89	90.1	83.2	81.2	88.2	87
5 stories	88.1	81.3	83.2	87.5	86	89.1	85.6
8 stories	82.2	88	86	81.9	84.1	79.6	84.8
11 stories	70.1	76.2	79.2	69.8	76.3	76	74.5
14 stories	81.1	78.9	76	81.3	78.8	72	77

Table 10 - The percentage of reduced quantity of lateral displacement of the base isolation's upper level in structures with support under F.F earthquakes

Earthquake / Structure	Imperial Valley	Loma Prieta	Tabas	Kobe	Chi Chi	Kocaeli	Northridge
3 stories	92.2	88.1	90	78	89.3	84.4	88
5 stories	90.4	89.7	92.2	83.3	88.9	91.1	90.3
8 stories	84.8	91.1	86.8	90.1	92.2	89.9	90.6
11 stories	37.6	41.2	39.3	80.3	40.1	36.1	44.7
14 stories	50.2	56.6	53.4	88.7	51.1	50.4	58.3

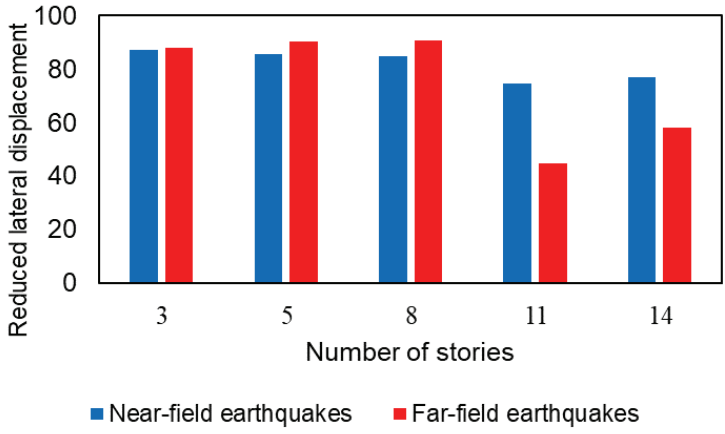

Fig. 14 - The percentage of reduced quantity of lateral displacement of the base isolation's upper level in structures with support under earthquakes

Table 11 - The average absolute value of base shear of the base isolation's upper level in structures with and without rigid support under N.F and F.F earthquakes (kg)

Field / Structure	N.F		F.F	
	With rigid support	Without rigid support	With rigid support	Without rigid support
3 stories	41500	9950	52100	13200
5 stories	51100	19100	61300	20250
8 stories	54050	19050	61500	19600
11 stories	125100	90200	135300	115400
14 stories	133000	99100	130550	105200

Table 12 - The percentage of reduced quantity of base shear of the base isolation's upper level in structures with support under N.F earthquakes

Earthquake / Structure	Chi Chi	San Fernando	Palm springs	Kocaeli	Gazil	Whittier narrows	Northridge
3 stories	78.8	80.1	76.6	82.4	75.3	79.9	78
5 stories	64.1	60.6	64.9	65.5	68	62.1	64
8 stories	47	42	41.1	48.8	44	48.3	45
11 stories	24.4	26	24.4	29.9	28.1	22.2	26
14 stories	26	22.6	20.1	30.7	28.5	23.1	25

Table 13 - The percentage of reduced quantity of the base shear of the base isolation upper level in structures with support under F.F earthquakes

Earthquake / Structure	Imperial Valley	Loma Prieta	Tabas	Kobe	Chi Chi	Kocaeli	Northridge
3 stories	78.2	69.2	65.9	73	78.8	66.6	71
5 stories	59	71.1	67.7	58.8	64.1	68.8	66
8 stories	63.3	54	50.1	58.8	57	52.2	55
11 stories	11	16.9	21.2	12.6	14.4	10.1	15
14 stories	13.6	17	26.6	18.9	17	21.1	19

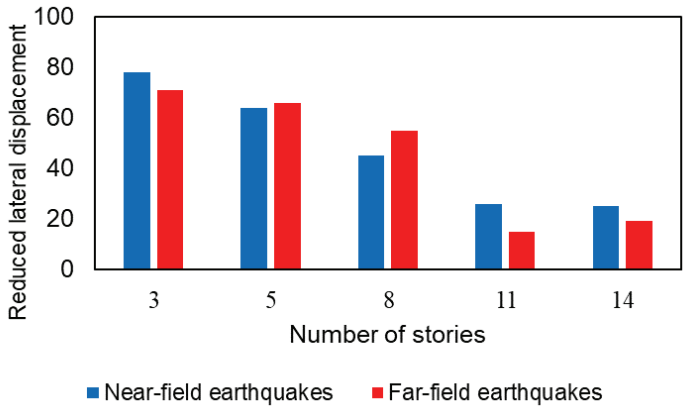

Fig. 15 - The percentage of reduced quantity of the base shear of the base isolation upper level in structures with support under earthquakes

According to the results, there are four main advantages for the structures with horizontal crosswise dissipators connected to the vertex of central rigid support. The first significant influence of support structures possessing dissipators in N.F earthquakes is the reduction of the displacement of the base isolation's upper level and reducing the base shear both in N.F and F.F earthquakes, particularly in buildings with lower numbers of stories.

As seen in Fig. 16, Fig. 17 and Fig. 18 the stories' velocity average in the structures are obtained as an average of F.F and N.F earthquakes records.

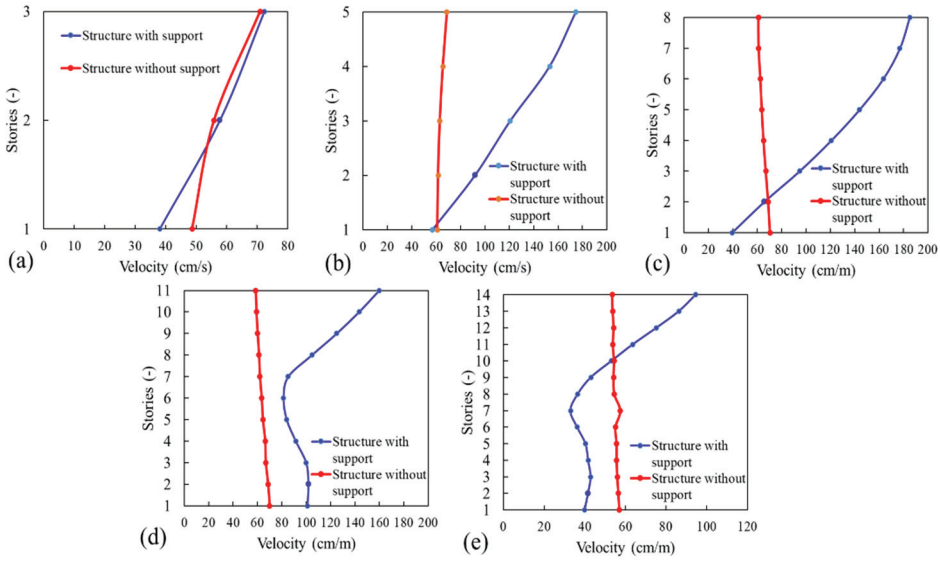

Fig. 16 - The F.F earthquake's stories velocity average for (a) 3-story, (b) 5-story, (c) 8-story, (d) 11-story, and (e) 14-story structure

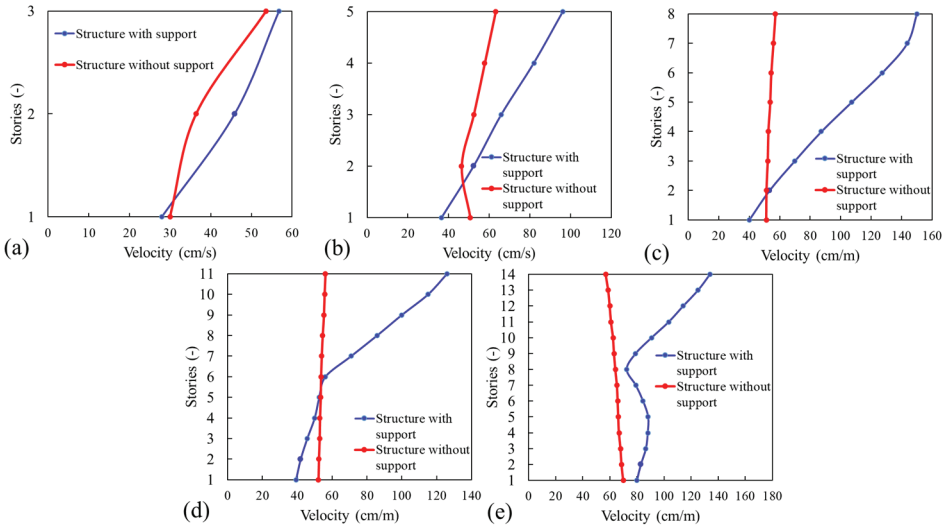

Fig. 17 - The N.F earthquake's stories velocity average for (a) 3-story, (b) 5-story, (c) 8-story, (d) 11-story, and (e) 14-story structure

Table 14 - The average absolute value of velocity of the base isolation upper level in structures with and without rigid support in N.F and F.F earthquakes

Field / Structure	N.F		F.F	
	With rigid support	**Without rigid support**	**With rigid support**	**Without rigid support**
3 stories	30	43.57	58.53	56.07
5 stories	54.08	66.66	63.94	119.48
8 stories	53.59	97.33	64.98	123.78
11 stories	53.76	71.21	63.66	107.08
14 stories	54.93	52.08	64.12	87.19

Table 15 - The percentage of average conversion of velocities in structures with support under N.F earthquakes

Earthquake / Structure	Chi Chi	San Fernando	Palm springs	Kocaeli	Gazil	Whittier narrows	Northridge
3 stories	5.7	11.1	8.8	9.1	6.6	8.2	8.2
5 stories	20.5	17.7	14.4	16.3	24.1	20.2	18.9
8 stories	50.1	39.8	42.7	43.3	51	53.3	45
11 stories	21	19	31.9	22.2	30.1	19.6	24.3
14 stories	-7	-7.9	-3.1	-4.7	6.8	-2.4	-5.2

Table 16 - The percentage of average conversion of velocities in structures with support under F.F earthquakes

Earthquake / Structure	Imperial Valley	Loma Prieta	Tabas	Kobe	Chi Chi	Kocaeli	Northridge
3 stories	4.9	-5.9	-8	-4.7	5.6	-6.8	-4.2
5 stories	46	49.2	51	46.5	49.1	53.9	46.5
8 stories	49	39.8	51.1	33.3	54.4	61.6	48
11 stories	38.9	43.6	39	45.6	40.3	44.3	40.6
14 stories	36.3	27.8	30.9	27.8	31.1	33.6	31.4

The intention behind using base isolation system is to reduce the ground acceleration in the horizontal direction. This is achieved by adding stiffness between the building and its base leading to a lower frequency. The first dynamic mode of the isolated structure shows deformation in the isolators only. However, the higher modes affect the building itself. The purpose of the isolator is to deflect the earthquake energy. Damping is a favorable parameter in isolators, but too much damping could become an issue as well since it can be acting as a conduit for energy to be induced in the higher modes of the isolated structure. Obviously, by controlling the isolators' displacement, the amount of velocity and acceleration of the stories increases. However, using dissipators in N.F earthquakes leads to a drop in the velocity of the structures, particularly in tall structures. Under far-field earthquakes, similar effects are found.

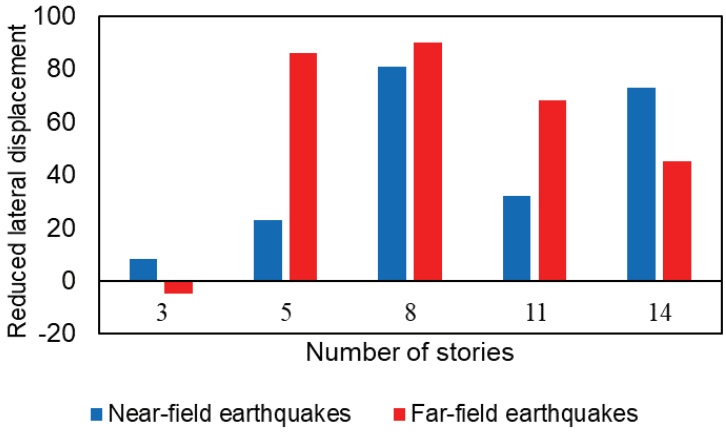

Fig. 18 - The percentage of average conversion of velocities in structures with support under earthquakes

According to Fig. 19, 20, and 21 and Table 17, 18, and 19, these structures' response is obtained as N.F and F.F scaled earthquakes records. The average conversion of the stories acceleration is presented in the following table and figures.

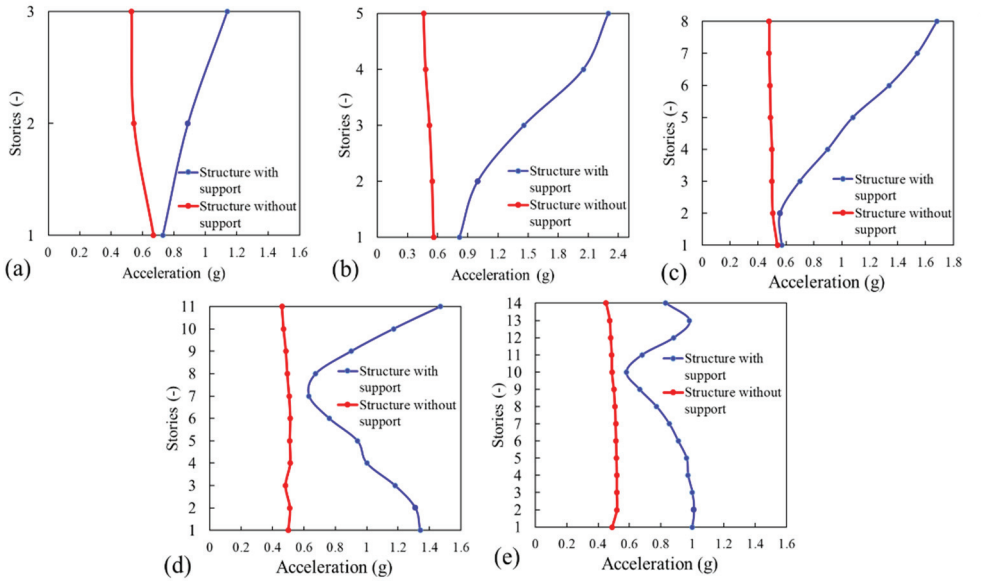

Fig. 19 - The F.F earthquake's stories acceleration average for (a) 3-story, (b) 5-story, (c) 8-story, (d) 11-story, and (e) 14-story structure

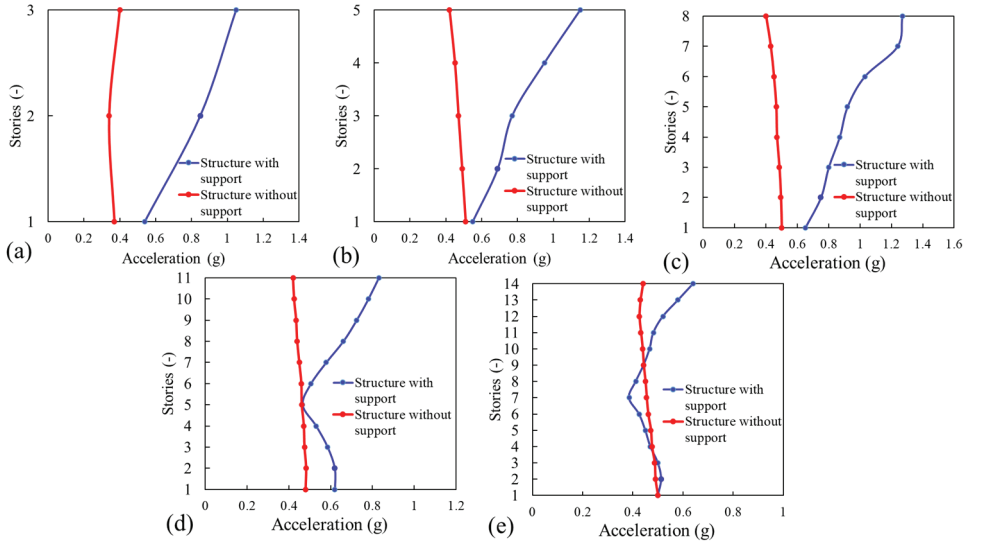

Fig. 20 - The N.F earthquake's stories acceleration average for (a) 3-story, (b) 5-story, (c) 8-story, (d) 11-story, and (e) 14-story structure

Table 17 - The average absolute value of accelerations of the base isolation upper level in structures with and without rigid support in N.F and F.F earthquakes

Field / Structure	N.F		F.F	
	With rigid support	Without rigid support	With rigid support	Without rigid support
3 stories	0.37	0.813	0.582	0.92
5 stories	0.468	0.822	0.513	1.526
8 stories	0.462	0.941	0.498	1.046
11 stories	0.455	0.627	0.494	1.034
14 stories	0.457	0.485	0.499	0.864

Table 18 - The percentage of average conversion of accelerations in rigid-support structures under N.F earthquakes

Earthquake / Structure	Chi Chi	San Fernando	Palm springs	Kocaeli	Gazil	Whittier narrows	Northridge
3 stories	46.7	67.8	48.8	44.1	49.9	68.1	54.5
5 stories	41.8	51.1	38.4	46.1	37.9	44.2	43
8 stories	57.9	60.6	56.6	43.8	62.6	57.1	56.3
11 stories	28.8	22.6	29.8	23.4	29.2	30.8	27.5
14 stories	4	7.1	6.7	6.1	4.9	5.7	5.7

Table 19 - The percentage of average conversion of accelerations in rigid-support structures under F.F earthquakes

Earthquake / Structure	Imperial Valley	Loma Prieta	Tabas	Kobe	Chi Chi	Kocaeli	Northridge
3 stories	38.7	43.9	39.9	35.3	39	23.3	36.8
5 stories	67.7	61.1	71.4	60.4	69	68.6	66.4
8 stories	57.1	49	59	55.7	45	49	52.4
11 stories	49.1	58.6	48.7	49.8	49	59	52.2
14 stories	40.1	45.3	47.1	32.4	58.7	29.3	42.3

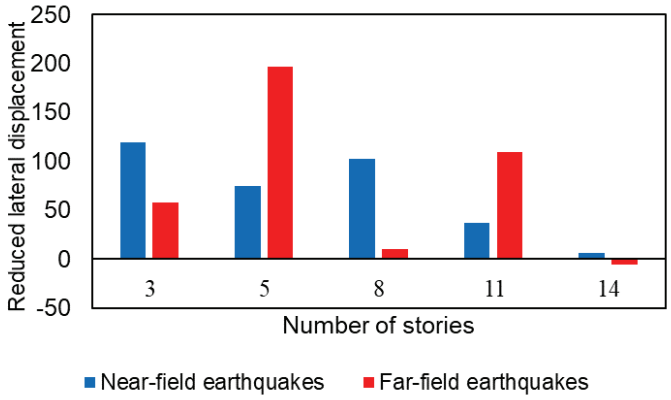

Fig. 21 - The percentage of average conversion of accelerations in rigid-support structures under earthquakes

The acceleration in N.F earthquakes is proved to be decreased by using the dissipators. Also, alteration of the structure's first modal shape from shear to torsional is achieved. This is significant in decreasing the modal mass effect on the structure's first action. Furthermore, it seems that the danger of buildings collapse has decreased dramatically in N.F earthquakes.

In Figs. 22 to 31, the hysteresis curve (force-displacement) of the upper level of the seismic isolators of buildings under study can be seen. The decreasing changes in the hysteresis curve of the structures equipped with the supporting structure are quite evident.

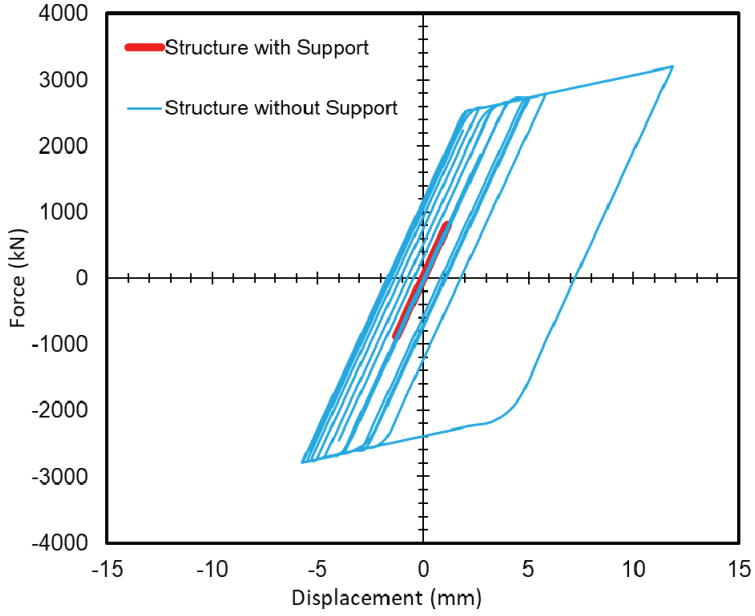

Fig. 22 - The F-D relation for the 3-strory structure in the far-field earthquake

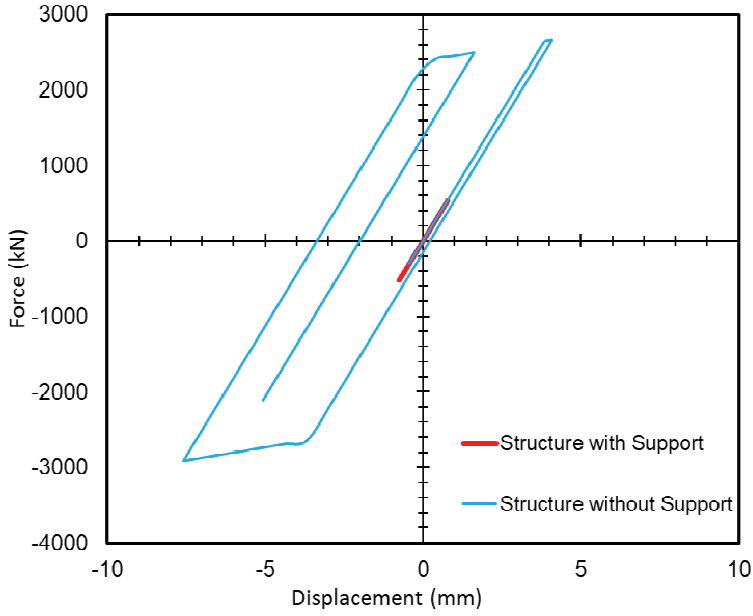

Fig. 23 - The F-D relation for the 3-strory structure in the near-field earthquake

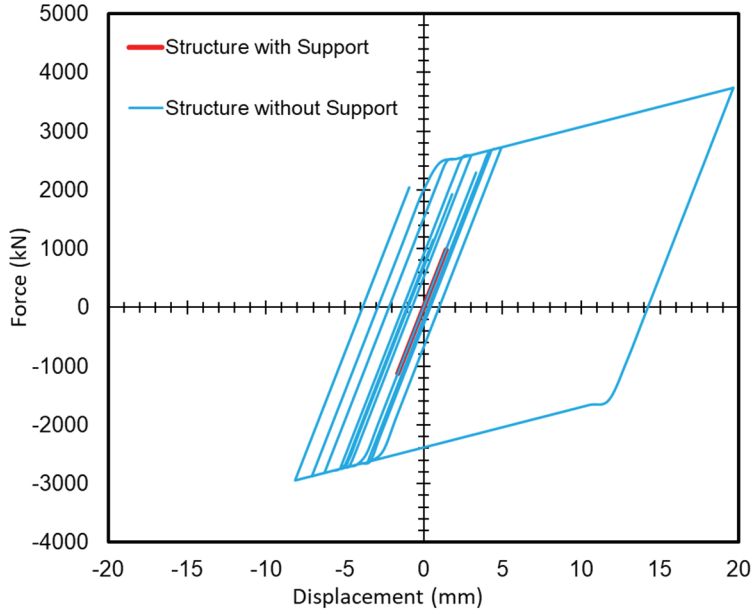

Fig. 24 - The F-D relation for the 5-strory structure in the far-field earthquake

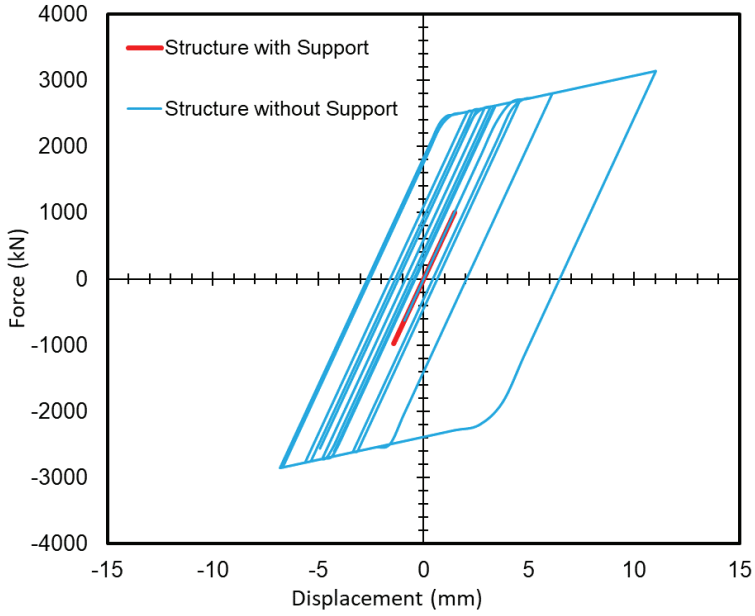

Fig. 25 - The F-D relation for the 5-strory structure in the near-field earthquake

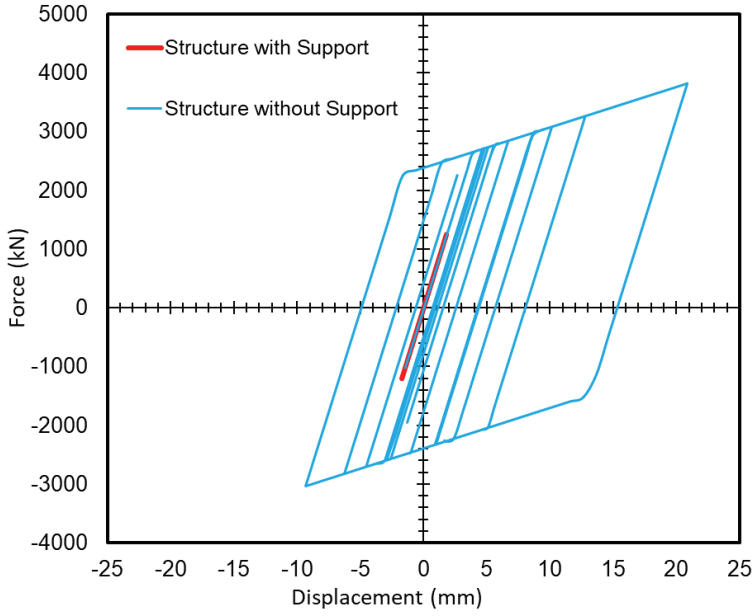

Fig. 26 - The F-D relation for the 8-strory structure in the far-field earthquake

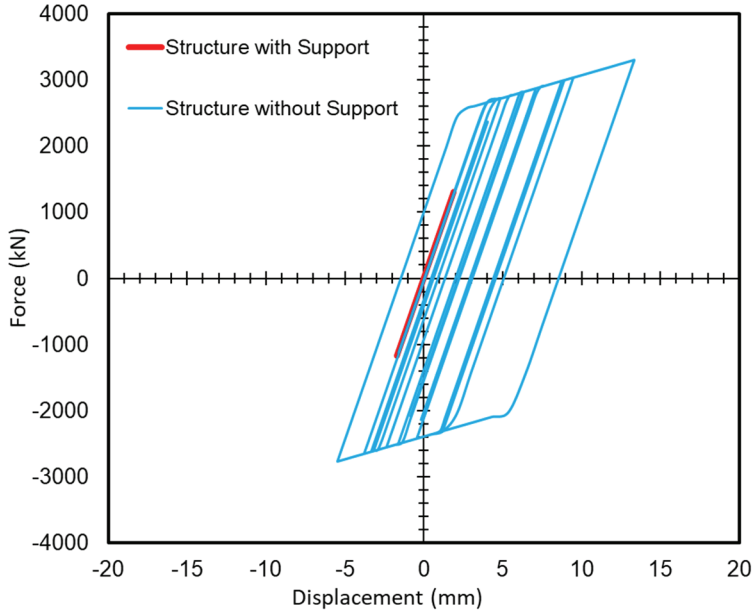

Fig. 27 - The F-D relation for the 8-strory structure in the near-field earthquake

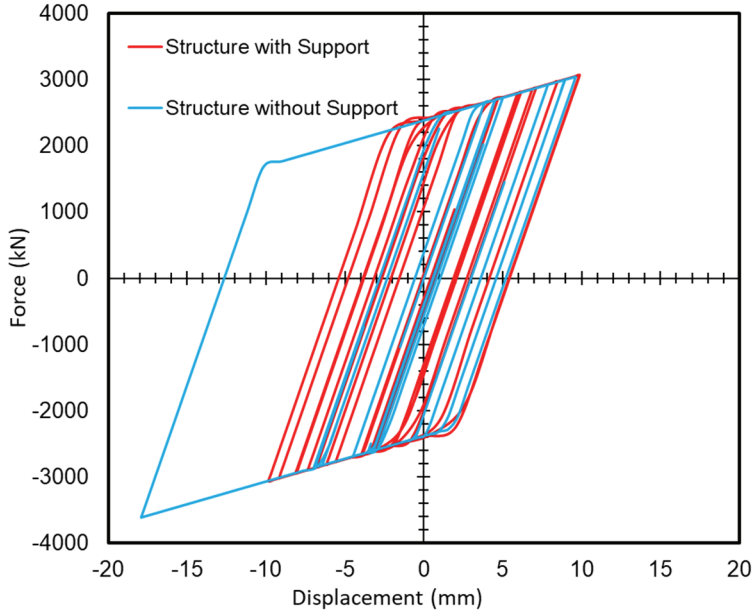

Fig. 28 - The F-D relation for the 11-strory structure in the far-field earthquake

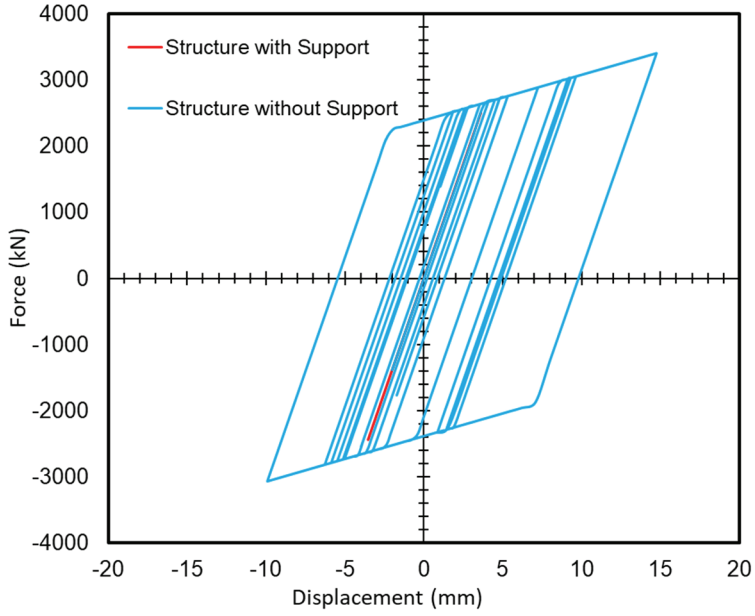

Fig. 29 - The F-D relation for the 11-strory structure in the near-field earthquake

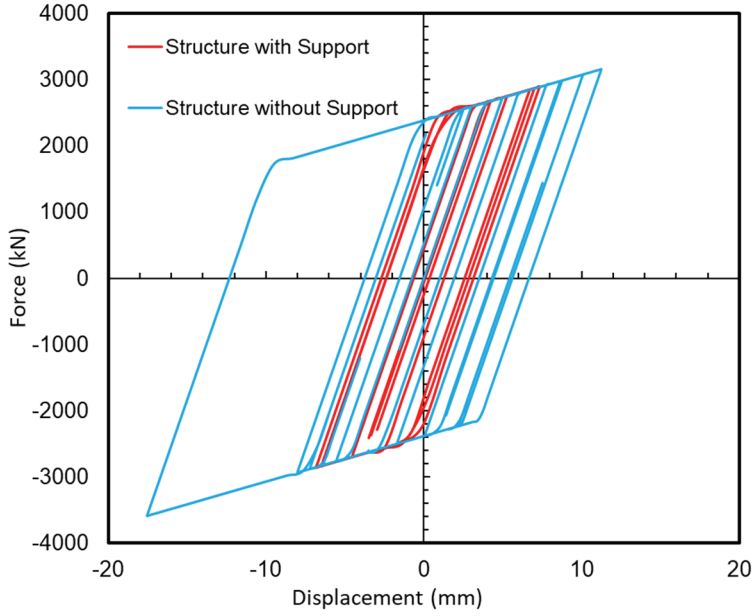

Fig. 30 - The F-D relation for the 14-strory structure in the far-field earthquake

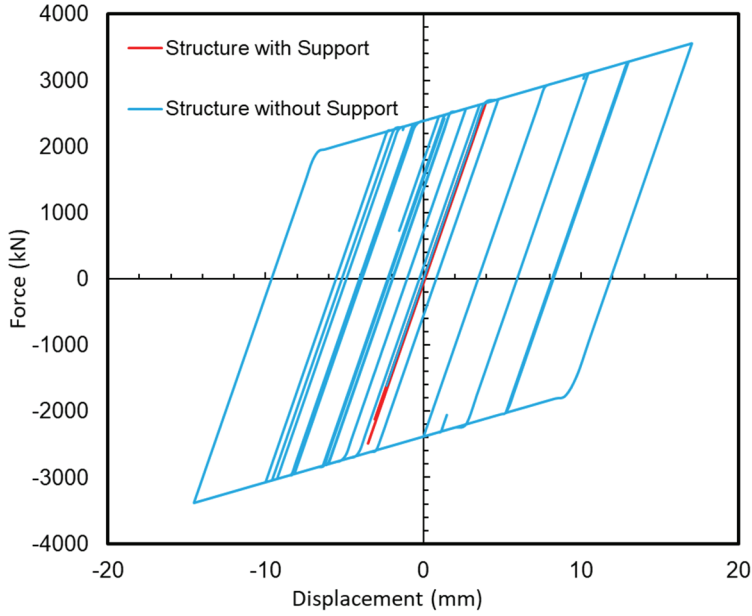

Fig. 31 - The F-D relation for the 14-strory structure in the near-field earthquake

5. CONCLUSION

Base isolation is the only anti-seismic technique that is able to save the building and its contents. In F.F earthquakes, acceptable performance is observed from the isolator, but in case of N.F ground motions they do not seem as helpful. Furthermore, utilizing such system is extremely expensive, which is in a controversy with the fundamental purpose of using seismic isolators. Normally, designing the base isolation, the destructive impacts of an earthquake are reduced, while prolonging the life of a structure and making a rigid body for the structures. Though the mentioned features can be improved through a base isolation system, regarding a near-field earthquake, a considerable drop may occur in the stability of the structures leading to the overturn and destruction of the building. According to the former studies, critical lateral displacement may be experienced by a building equipped with an isolator, and it could result in the overturn of the structure. A safe method is presented in the present study as a remedy to the stated problem to decrease the base isolation lateral displacement under near-field earthquakes. A supportive structure is designed, which is connected to the roof of the building by a viscous damper in a crosswise manner. It is also rigidly connected to the building's base. According to the results, there are five main advantages of implementing the proposed technique:

- Hybrid buildings consisting of base isolation and viscous dampers require a large number of dampers on each floor, and the sum total of the dampers used in those buildings, due to the high cost of viscous dampers and the high cost of servicing and maintaining these dampers, it creates a very high cost for the builders of those

buildings, perhaps this very high cost has been imposed, which has prevented the generalization of the use of these types of buildings.

- The biggest achievement of this research is the use of 4 viscous dampers in each building, which has significantly reduced the staggering costs of hybrid buildings.
- In all structures exposed to N.F earthquakes, the displacement of the base isolation is reduced significantly.
- It was proved that the base shear was decreased substantially under N.F earthquakes.
- By limiting the lateral displacement of the isolators, the floor velocity of all structures increased, with the least amount of velocity increase occurring in short and tall structures.
- By controlling the isolators' displacement, the amount of acceleration of the stories increases, with the least amount of acceleration increase occurring in tall structures.
- The structure's first modal shape was changed from shear to torsional.

Based on these benefits, the application of LRB isolators eliminated the impacts of N.F earthquakes. Furthermore, the present technique could decrease the near-field earthquake-caused mortality rates. Similarly, by utilizing the proposed technique, the damage to the property is also reduced considerably.

Nomenclature

A_{pb}	Area of the lead core
A_r	Cross-sectional area of rubber
a_q	Relative acceleration of the nth degree of freedom
c	Coefficient of velocity
C_{eff}	Effective damping coefficient
D	The isolator diameter
D_y	Yield displacement
d	The lead core diameter
ED	Area of the hysteretic loop
F_D	Viscous damper force
F_m	Force
F_y	Yield force
fL	Constant
G	Shear modulus

k_e	Elastic stiffness
k_{eff}	Effective stiffness
k_p	Yielded stiffness in isolation
M	Overall mass of the system
m_q	Mass of the nth degree of freedom
n	The number of rubber layers
Q	Strength
T^{iso}	Fundamental isolation period
V_c	Relative velocity

Greek Letters

Δ	Displacement
$\sigma_{y_{pb}}$	Yield strength of the lead core
ζ_{eff}	Damping ratio

References

[1] Erkus B, Johnson EA. Smart base-isolated benchmark building part III: a sample controller for bilinear isolation. Structural Control and Health Monitoring: The Official Journal of the International Association for Structural Control and Monitoring and of the European Association for the Control of Structures. 2006 Mar; 13(2-3):605-25; https://doi.org/10.1002/stc.101.

[2] Nagarajaiah S, Narasimhan S. Smart base isolated benchmark building part II: sample controllers for linear and friction isolation. InProc. 16th ASCE Engineering Mechanics Conference, July 2003 (pp. 16-18).

[3] He WL, Agrawal AK. Applications of several semi-active control systems to the benchmark base-isolated building. In Proceedings of the ASCE Engineering Mechanics Conference 2004 Jun.

[4] Huang, S., Huang, M., & Lyu, Y. (2021). Seismic performance analysis of a wind turbine with a monopile foundation affected by sea ice based on a simple numerical method. Engineering applications of computational fluid mechanics, 15(1), 1113-1133.

[5] Feng, Y., Zhang, B., Liu, Y., Niu, Z., Dai, B., Fan, Y., Chen, X. (2021). A 200-225-GHz Manifold-Coupled Multiplexer Utilizing Metal Wave guides. IEEE Transactions on Microwave Theory and Techniques, 1.

[6] Kim SB, Spencer Jr BF, Yun CB. Sliding mode fuzzy control for smart base isolated building. In17th ASCE Engineering Mechanics Conference (EM2004), Newark, USA 2004 Jun 13.

[7] Bai, Y., Nardi, D. C., Zhou, X., Picón, R. A., & Flórez-López, J. (2021). A new comprehensive model of damage for flexural subassemblies prone to fatigue. Computers & Structures, 256, 106639.

[8] Reigles D, Symans MD. Application of supervisory fuzzy logic controller to the base-isolated benchmark structure. In Proceedings of the ASCE Engineering Mechanics Conference 2004 Jun.

[9] Zhang, C., 2022. The active rotary inertia driver system for flutter vibration control of bridges and various promising applications. *Science China Technological Sciences*, pp.1-16.

[10] Choi KM, Jung HJ, Lee IW. Fuzzy control strategy for seismic response reduction of smart base isolated benchmark building. In17th ASCE Engineering Mechanics Conference 2004.

[11] Guo, Y., Yang, Y., Kong, Z., He, J., & Wu, H. (2022). Development of Similar Materials for Liquid-Solid Coupling and Its Application in Water Outburst and Mud Outburst Model Test of Deep Tunnel. Geofluids, 2022.

[12] Jung HJ, Moon YJ, Jang JE, Spencer BF. Robust hybrid control systems for seismic protection of benchmark base isolated building. Proceedings of the ASCE Engineering Mechanics Conference, June 2004, Newark, DE, CD-ROM.

[13] Huang, H., Li, M., Yuan, Y. and Bai, H., 2023. Experimental Research on the Seismic Performance of Precast Concrete Frame with Replaceable Artificial Controllable Plastic Hinges. *Journal of Structural Engineering*, *149*(1), p.04022222.

[14] Skinner RI, McVerry GH, Robinson WH. An Introduction to Seismic Isolation. Wiley, 1993 (ISBN: 047193433).

[15] Zhang, C. and Ali, A., 2021. The advancement of seismic isolation and energy dissipation mechanisms based on friction. *Soil Dynamics and Earthquake Engineering*, *146*, p.106746.

[16] Kakolvand, H., Ghazi, M., Mehrparvar, B. and Parvizi, S., 2022. Experimental and numerical study of a new proposed seismic isolator using steel rings (SISR). *Journal of Earthquake Engineering*, *26*(8), pp.4000-4029.

[17] Öncü-Davas, S. and Alhan, C., 2019. Reliability of semi-active seismic isolation under near-fault earthquakes. *Mechanical Systems and Signal Processing*, *114*, pp.146-164.

[18] Jiang, L., Zhong, J. and Yuan, W., 2020, October. The pulse effect on the isolation device optimization of simply supported bridges in near-fault regions. In *Structures* (Vol. 27, pp. 853-867). Elsevier.

[19] Wu, L.Y., Wang, Z., Ma, D., Zhang, J.W., Wu, G., Wen, S., Zha, M. and Wu, L., 2022. A continuous damage statistical constitutive model for sandstone and mudstone based on triaxial compression tests. *Rock Mechanics and Rock Engineering*, *55*(8), pp.4963-4978.

[20] Wu, L.Y., Ma, D., Wang, Z. and Zhang, J.W., 2022. Prediction and prevention of mining-induced water inrush from rock strata separation space by 3D similarity simulation testing: a case study of Yuan Zigou coal mine, China. *Geomechanics and Geophysics for Geo-Energy and Geo-Resources*, *8*(6), p.202.

[21] Kelly JM. Earthquake-Resistant Design with Rubber, 2nd ed. Springer: New York, 1997 (ISBN: 3540761314).

[22] Huang, Y., Zhang, W. and Liu, X., 2022. Assessment of diagonal macrocrack-induced debonding mechanisms in FRP-strengthened RC beams. *Journal of Composites for Construction*, *26*(5), p.04022056.

[23] Heaton TH, Hall JF, Wald DJ, Halling MW. Response of high-rise and base-isolated buildings to a hypothetical M w 7.0 blind thrust earthquake. Science. 1995 Jan 13; 267(5195):206-11; https://doi.org/10.1126/science.267.5195.206.

[24] Chen, J., Tong, H., Yuan, J., Fang, Y. and Gu, R., 2022. Permeability prediction model modified on Kozeny-Carman for building foundation of clay soil. *Buildings*, *12*(11), p.1798.

[25] Nagarajaiah S, Ferrell K. Stability of elastomeric seismic isolation bearings. Journal of Structural Engineering. 1999 Sep; 125(9):946-54; https://ascelibrary.org/doi/abs/10.1061/(ASCE)0733-9445(1999)125:9(946).

[26] Gu, M., Cai, X., Fu, Q., Li, H., Wang, X. and Mao, B., 2022. Numerical analysis of passive piles under surcharge load in extensively deep soft soil. *Buildings*, *12*(11), p.1988.

[27] Soong TT. Active Structural Control: Theory and Practice. Wiley: New York, ISBN 0-470-21670-0, 1991.

[28] Symans MD, Constantinou MC. Semi-active control systems for seismic protection of structures: a state-of-the-art review. Engineering structures. 1999 Jun 1; 21(6):469-87; https://doi.org/10.1016/S0141-0296(97)00225-3.

[29] Housner G, Bergman LA, Caughey TK, Chassiakos AG, Claus RO, Masri SF, Skelton RE, Soong TT, Spencer BF, Yao JT. Structural control: past, present, and future. Journal of engineering mechanics. 1997 Sep; 123(9):897-971; https://ascelibrary.org/doi/abs/10.1061/(ASCE)0733-9399(1997)123:9(897).

[30] Deng, E.F., Zhang, Z., Zhang, C.X., Tang, Y., Wang, W., Du, Z.J. and Gao, J.P., 2023. Experimental study on flexural behavior of UHPC wet joint in prefabricated multi-girder bridge. *Engineering Structures*, *275*, p.115314.

[31] Soong TT, Spencer Jr BF. Supplemental energy dissipation: state-of-the-art and state-of-the-practice. Engineering structures. 2002 Mar 1; 24(3):243-59; https://doi.org/10.1016/S0141-0296(01)00092-X.

[32] Zhai, S.Y., Lyu, Y.F., Cao, K., Li, G.Q., Wang, W.Y. and Chen, C., 2023. Seismic behavior of an innovative bolted connection with dual-slot hole for modular steel buildings. *Engineering Structures*, *279*, p.115619.

[33] Spencer Jr BF, Nagarajaiah S. State of the art of structural control. Journal of structural engineering. 2003 Jul; 129(7):845-56; https://ascelibrary.org/doi/abs/10.1061/(ASCE)0733-9445(2003)129:7(845).

[34] Wu, L., Ma, D., Wang, Z., Zhang, J., Zhang, B., Li, J., Liao, J. and Tong, J., 2023. An deep CNN-based constitutive model for describing of statics characteristics of rock materials. *Engineering Fracture Mechanics*, p.109054.

[35] Yang JN, Wu JC, Agrawal AK. Sliding mode control for nonlinear and hysteretic structures. Journal of Engineering Mechanics. 1995 Dec; 121(12):1330-9; https://ascelibrary.org/doi/abs/10.1061/(ASCE)0733-9399(1995)121:12(1330).

[36] Wang, G., Zhao, B., Wu, B., Wang, M., Liu, W., Zhou, H., Zhang, C., Wang, Y., Han, Y. and Xu, X., 2022. Research on the macro-mesoscopic response mechanism of multisphere approximated heteromorphic tailing particles. *Lithosphere*, *2022*(Special 10).

[37] Yang JN, Wu JC, Reinhorn AM, Riley M. Control of sliding-isolated buildings using sliding-mode control. Journal of Structural Engineering. 1996 Feb; 122(2):179-86; https://ascelibrary.org/doi/abs/10.1061/(ASCE)0733-9445(1996)122:2(179).

[38] Nagarajaiah S. Fuzzy controller for structures with hybrid isolation system. InProc. First World Conf. Struct. Control, Los Angeles, CA 1994 (pp. 67-76).

[39] Wang, G., Zhao, B., Wu, B., Zhang, C. and Liu, W., 2023. Intelligent prediction of slope stability based on visual exploratory data analysis of 77 in situ cases. *International Journal of Mining Science and Technology*, *33*(1), pp.47-59.

[40] Nagarajaiah S, Riley MA, Reinhorn A. Control of sliding-isolated bridge with absolute acceleration feedback. Journal of engineering Mechanics. 1993 Nov; 119(11):2317-32; https://ascelibrary.org/doi/abs/10.1061/(ASCE)0733-9399(1993)119%3A11(2317).

[41] Yang JN, Agrawal AK. Semi-active hybrid control systems for nonlinear buildings against near-field earthquakes. Engineering structures. 2002 Mar 1; 24(3):271-80; https://doi.org/10.1016/S0141-0296(01)00094-3.

[42] Yang JN. Application of optimal control theory to civil engineering structures. Journal of the engineering Mechanics Division. 1975 Dec;101(6):819-38; https://ascelibrary.org/doi/abs/10.1061/JMCEA3.0002075.

[43] Li, J., Cheng, F., Lin, G. and Wu, C., 2022. Improved hybrid method for the generation of ground motions compatible with the multi-damping design spectra. *Journal of Earthquake Engineering*, pp.1-27.

[44] Yang JN, Wu JC, Agrawal AK, Li Z. Sliding mode control for seismic-excited linear and nonlinear civil engineering structures. National Center for Earthquake Engineering Research, Technical Report NCEER-94-0017. 1994 Jun 21; https://ascelibrary.org/doi/abs/10.1061/%28ASCE%290733-9399%281995%29121%3A12%281386%29.

[45] Huang, S., Lyu, Y., Sha, H., & Xiu, L. (2021). Seismic performance assessment of unsaturated soil slope in different groundwater levels. Landslides, 18(8), 2813-2833.

[46] Panariello GF, Betti R, Longman RW. Optimal structural control via training on ensemble of earthquakes. Journal of engineering mechanics. 1997 Nov; 123(11):1170-9; https://ascelibrary.org/doi/abs/10.1061/(ASCE)0733-9399(1997)123:11(1170).

[47] Yoshioka H, Ramallo JC, Spencer Jr BF. "Smart" base isolation strategies employing magnetorheological dampers. Journal of engineering mechanics. 2002 May; 128(5):540-51; https://ascelibrary.org/doi/abs/10.1061/(ASCE)0733-9399(2002)128:5(540).

[48] Ramallo JC, Johnson EA, Spencer Jr BF. "Smart" base isolation systems. Journal of Engineering Mechanics. 2002 Oct; 128(10):1088-99; https://ascelibrary.org/doi/abs/10.1061/(ASCE)0733-9399(2002)128:10(1088).

[49] Alimoradi, H., Eskandari, E., Pourbagian, M. and Shams, M., 2022. A parametric study of subcooled flow boiling of Al2O3/water nanofluid using numerical simulation and artificial neural networks. *Nanoscale and Microscale Thermophysical Engineering*, *26*(2-3), pp.129-159.

[50] Soong TT, Grigoriu M. Random vibration of mechanical and structural systems. NASA STI/Recon Technical Report A. 1993; 93:14690; https://ui.adsabs.harvard.edu/abs/1993STIA...9314690S/abstract.

[51] He W. Smart energy dissipation systems for protection of civil infrastructures from near-field earthquakes. City University of New York; 2003; https://www.proquest.com/openview/0171ba4787fee2145cae0e21240e3fa2/1?pq-origsite=gscholar&cbl=18750&diss=y.

[52] He WL, Agrawal AK. An analytical model for ground motion pulses during near-field earthquakes for the design of smart protective systems. Journal of Structural Engineering (ASCE). 2005.

[53] Eskandari, E., Alimoradi, H., Pourbagian, M. and Shams, M., 2022. Numerical investigation and deep learning-based prediction of heat transfer characteristics and bubble dynamics of subcooled flow boiling in a vertical tube. *Korean Journal of Chemical Engineering*, *39*(12), pp.3227-3245.

[54] He WL, Agrawal AK. Passive and hybrid control systems for seismic protection of a benchmark cable-stayed bridge. Structural Control and Health Monitoring: The Official Journal of the International Association for Structural Control and Monitoring and of the European Association for the Control of Structures. 2007 Feb; 14(1):1-26; https://doi.org/10.1002/stc.81.

[55] Xu Z. Design and assessment of seismic protective systems for near-field ground motions. City University of New York; 2007; https://www.proquest.com/openview/d72dee3441cd311cd30c019d1718430a/1?pq-origsite=gscholar&cbl=18750.

[56] Agrawal, A.K., Xu, Z. and He, W.L., 2006. Ground motion pulse-based active control of a linear base-isolated benchmark building. *Structural Control and Health Monitoring: The Official Journal of the International Association for Structural Control and Monitoring and of the European Association for the Control of Structures*, *13*(2-3), pp.792-808.

[57] Xu, Z., Agrawal, A.K. and Yang, J.N., 2006. Semi-active and passive control of the phase I linear base-isolated benchmark building model. *Structural Control and Health Monitoring: The Official Journal of the International Association for Structural Control and Monitoring and of the European Association for the Control of Structures*, *13*(2-3), pp.626-648.

[58] Özuygur, A.R. and Noroozinejad Farsangi, E., 2021. Influence of pulse-like near-fault ground motions on the base-isolated buildings with LRB devices. *Practice Periodical on Structural Design and Construction*, *26*(4), p.04021027.

[59] AISC code, Specification for Structural Steel Buildings (ANSI/AISC 360-05), American Institute of Steel Construction, Inc., Chicago, IL., USA, 2005.

[60] International Herald Tribune, UN Says Half the World's Population will Live in Urban Areas by End of 2008, Associated Press, New York, NY, USA, 2009.

[61] Maffei J, Yuen N. Seismic performance and design requirements for high-rise buildings. Structural Magazine. 2007 Apr 28:28-32.

[62] Mehmood T, Warnitchai P, Suwansaya P. Seismic evaluation of tall buildings using a simplified but accurate analysis procedure. Journal of Earthquake Engineering. 2018 Mar 16; 22(3):356-81; https://doi.org/10.1080/13632469.2016.1224742.

[63] Code, U.B. UBC-97 in Structural Engineering Design Provisions, International Conference of Building Officials, Whittier, CA, USA, 1997.

[64] Prestandard FE. commentary for the seismic rehabilitation of buildings (FEMA356). Washington, DC: Federal Emergency Management Agency. 2000;7(2).

[65] Comartin CD. Seismic evaluation and retrofit of concrete buildings. Seismic Safety Commission, State of California; 1996.

[66] Soleimani S, Aziminejad A, Moghadam AS. Approximate two-component incremental dynamic analysis using a bidirectional energy-based pushover procedure. Engineering Structures. 2018 Feb 15; 157:86-95; https://doi.org/10.1016/j.engstruct.2017.11.056.

[67] Panyakapo P. Cyclic pushover analysis procedure to estimate seismic demands for buildings. Engineering Structures. 2014 May 1; 66:10-23; https://doi.org/10.1016/j.engstruct.2014.02.001.

[68] Poursha M, Khoshnoudian F, Moghadam AS. The extended consecutive modal pushover procedure for estimating the seismic demands of two-way unsymmetric-plan tall buildings under influence of two horizontal components of ground motions. Soil Dynamics and Earthquake Engineering. 2014 Aug 1; 63:162-73; https://doi.org/10.1016/j.soildyn.2014.02.001.

[69] Belejo A, Bento R. Improved modal pushover analysis in seismic assessment of asymmetric plan buildings under the influence of one and two horizontal components of ground motions. Soil Dynamics and Earthquake Engineering. 2016 Aug 1; 87:1-5; https://doi.org/10.1016/j.soildyn.2016.04.011.

[70] Soleimani S, Aziminejad A, Moghadam AS. Extending the concept of energy-based pushover analysis to assess seismic demands of asymmetric-plan buildings. Soil Dynamics and Earthquake Engineering. 2017 Feb 1; 93:29-41; https://doi.org/10.1016/j.soildyn.2016.11.014.

[71] Najam FA, Qureshi MI, Warnitchai P, Mehmood T. Prediction of nonlinear seismic demands of high-rise rocking wall structures using a simplified modal pushover analysis procedure. The Structural Design of Tall and Special Buildings. 2018 Oct 25; 27(15):e1506; https://doi.org/10.1002/tal.1506.

[72] Brozovič M, Dolšek M. Envelope-based pushover analysis procedure for the approximate seismic response analysis of buildings. Earthquake Engineering & Structural Dynamics. 2014 Jan; 43(1):77-96; https://doi.org/10.1002/eqe.2333.

[73] Sürmeli M, Yüksel E. An adaptive modal pushover analysis procedure (VMPA-A) for buildings subjected to bi-directional ground motions. Bulletin of Earthquake Engineering. 2018 Nov;16(11):5257-77; https://doi.org/10.1007/s10518-018-0324-x.

[74] Goel RK, Chopra AK. Role of higher-"mode" pushover analyses in seismic analysis of buildings. Earthquake Spectra. 2005 Nov; 21(4):1027-41; https://doi.org/10.1193%2F1.2085189.

[75] Attard, T. and Dhiradhamvit, K., 2009. Application and design of lead-core base isolation for reducing structural demands in short stiff and tall steel buildings and highway bridges subjected to near-field ground motions. *Journal of Mechanics of Materials and Structures*, *4*(5), pp.799-817.

[76] Jangid, R.S. and Kelly, J.M., 2001. Base isolation for near-fault motions. Earthquake engineering & structural dynamics, 30(5), pp.691-707.

[77] Jangid, R.S., 2007. Optimum lead–rubber isolation bearings for near-fault motions. Engineering structures, 29(10), pp.2503-2513.

[78] Kelly JM. The role of damping in seismic isolation. Earthquake engineering & structural dynamics. 1999 Jan; 28(1):3-20; https://doi.org/10.1002/(SICI)1096-9845(199901)28:1%3C3::AID-EQE801%3E3.0.CO;2-D.

[79] HITEC (Highway Innovation Technology Evaluation Center). Evaluation Findings for R.J. Watson Inc. Sliding Isolation Bearings. Reston (VA): Technical evaluation report, ASCE, 1998.

[80] Uniform Building Code. International Conference of Building Officials. Whittier, CA. 1997.

[81] Kelly JM. Earthquake-resistant design with rubber. 2nd ed. London: Springer-Verlag; 1997.

[82] Lee, D. and Taylor, D.P., 2001. Viscous damper development and future trends. *The structural design of tall buildings*, *10*(5), pp.311-320.

[83] Makris, N., 1998. Viscous heating of fluid dampers. I: Small-amplitude motions. *Journal of engineering mechanics*, *124*(11), pp.1210-1216.

[84] Makris, N., Roussos, Y., Whittaker, A.S. and Kelly, J.M., 1998. Viscous heating of fluid dampers. II: Large-amplitude motions. *Journal of Engineering Mechanics*, *124*(11), pp.1217-1223.

[85] Soong, T.T. and Dargush, G.F., 1997. Passive Energy Dissipation Systems in Structural Engineering Wiley. *Chichester, UK*.

[86] Skinner RI, Robinson WH, McVerry GH. An introduction to seismic isolation. London: John Wiley and Sons; 1993.

[87] Makris N. Rigidity–plasticity–viscosity: Can electrorheological dampers protect base-isolated structures from near-source ground motions? Earthquake Engineering & Structural Dynamics. 1997 May; 26(5):571-91; https://doi.org/10.1002/(SICI)1096-9845(199705)26:5%3C571::AID-EQE658%3E3.0.CO;2-6.

[88] Jouneghani KT, Hosseini M, Rohanimanesh MS, Dehkordi MR. Evaluating main parameters effects of near-field earthquakes on the behavior of concrete structures with moment frame system. Advances in Science and Technology. Research Journal. 2018; 12(3); http://dx.doi.org/10.12913/22998624/74135.

[89] Jouneghani KT, Hosseini M, Rohanimanesh MS, Dehkordi MR. Dynamic behavior of steel frames with tuned mass dampers. Advances in Science and Technology. Research Journal. 2017; 11(2); http://dx.doi.org/10.12913/22998624/70763.

[90] Jouneghani KT, Rohanimanesh MS, Hosseini M, Raissi M. Reducing the lateral displacement of lead rubber bearing isolators under the near field earthquakes by crosswise dissipaters connected to rigid support structure: earthquake engineering. Stavební obzor-Civil Engineering Journal. 2021 Dec 31; 30(4); https://doi.org/10.14311/CEJ.2021.04.0066.

[91] Rodolfo Saragoni, G. and Hart, G.C., 1973. Simulation of artificial earthquakes. *Earthquake Engineering & Structural Dynamics*, *2*(3), pp.249-267.

[92] Hayashi, K., Fujita, K., Tsuji, M. and Takewaki, I., 2018. A simple response evaluation method for base-isolation building-connection hybrid structural system under long-period and long-duration ground motion. *Frontiers in Built Environment*, *4*, p.2.